ACS EARTH AND SPACE CHEMISTRY

http://pubs.acs.org/journal/aesccq

Article

The CU Airborne Solar Occultation Flux Instrument: Performance Evaluation during BB-FLUX

Natalie Kille, Kyle J. Zarzana, Johana Romero Alvarez, Christopher F. Lee, Jake P. Rowe, Benjamin Howard, Teresa Campos, Alan Hills, Rebecca S. Hornbrook, Ivan Ortega, Wade Permar, I Ting Ku, Jakob Lindaas, Ilana B. Pollack, Amy P. Sullivan, Yong Zhou, Carley D. Fredrickson, Brett B. Palm, Qiaoyun Peng, Eric C. Apel, Lu Hu, Jeffrey L. Collett, Jr., Emily V. Fischer, Frank Flocke, James W. Hannigan, Joel Thornton, and Rainer Volkamer*

Cite This: *ACS Earth Space Chem.* 2022, 6, 582−596

Read Online

ACCESS | Metrics & More | Article Recommendations | Supporting Information

ABSTRACT: Biomass burning is an important and increasing source of trace gases and aerosols relevant to air quality and climate. The Biomass Burning Flux Measurements of Trace Gases and Aerosols (BB-FLUX) field campaign deployed the University of Colorado Airborne Solar Occultation Flux (CU AirSOF) instrument aboard the University of Wyoming King Air research aircraft during the 2018 Pacific Northwest wildfire season (July−September). CU AirSOF tracks the sun even through thick smoke plumes using short-wave infrared wavelengths to minimize scattering from smoke particles, and uses Fourier transform infrared spectroscopy (FTS) to measure the column absorption of multiple trace gases at mid-infrared wavelengths. The instrument is described, characterized, and evaluated using colocated ground-based remote sensing and airborne in situ data sets. Vertical column density (VCD) measurements agree well with a colocated stationary high-resolution FTS for carbon monoxide (CO, slope within 2%), formaldehyde (HCHO, 3%), formic acid (HCOOH, 18%), ethane (C_2H_6, 4%), ammonia (NH_3, 4%), hydrogen cyanide (HCN, 10%), and peroxyacyl nitrate (PAN_{FTS}, 1%; we distinguish the molecule PAN from PAN_{FTS}, which includes similar molecules and is measured as a sum by FTS). Airborne VCD measurements are compared with in situ measurements aboard the NSF/NCAR C-130 aircraft during a coordinated mission to the Rabbit Foot Fire near Boise, Idaho by digesting VCDs into normalized excess column ratios (NEMRs). Column NEMRs from CU AirSOF, expressed as VCD enhancements over background and normalized to CO enhancements, are found to agree with the in situ NEMRs within 20% for HCHO, methanol (CH_3OH), ethylene (C_2H_4), C_2H_6, NH_3, and HCN and within 30−66% for HCOOH and PAN. CU AirSOF integrates over plume heterogeneity, is inherently calibrated, and provides an innovative, flexible, and quantitative tool to measure emission mass fluxes from wildfires.

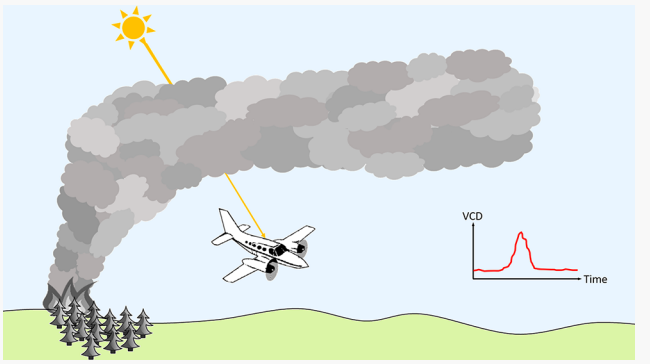

KEYWORDS: *emissions, wildfires, atmospheric chemistry, remote sensing, measurement technique, biomass burning, western United States*

Downloaded via UNIV OF COLORADO BOULDER on May 30, 2022 at 18:22:27 (UTC).
See https://pubs.acs.org/sharingguidelines for options on how to legitimately share published articles.

1. INTRODUCTION

Biomass burning is an important source of a variety of atmospheric trace gases.[1,2] The emissions from biomass burning, which includes wildfires in the western United States (U.S.), impact ecosystems, air quality, and human health (e.g., Chen et al.[3] or Reid et al.[4]). Uncertainties and discrepancies in emission inventories can have substantial impact on the conclusions drawn about the impacts fires have on air quality and climate (e.g., Carter et al.[5] or Bela et al.[6]). It therefore is increasingly important in the changing Earth system to be able to accurately quantify biomass burning emissions.[7] Plume injection heights are variable with smoke over North American biomes typically being lofted to altitudes between a few hundred meters to several kilometers above the terrain.[8] However, wildfires are frequently ignited in complex terrain without road access or with closed or impassable roads due to firefighting operations or weather conditions. There is therefore a need for flexible techniques to quantify emissions from wildfires, and the airborne Solar Occultation Flux (AirSOF) method has the potential to fill this gap in suborbital measurement capabilities. We describe an airborne adaptation

Special Issue: Mario Molina Memorial

Received: August 7, 2021
Revised: January 4, 2022
Accepted: January 4, 2022
Published: January 21, 2022

ACS Publications

© 2022 The Authors. Published by American Chemical Society

of the University of Colorado (CU) mobile SOF instrument[9] and evaluate the CU AirSOF performance in actual wildfire plumes.

The SOF technique uses a solar tracker coupled to a Fourier transform infrared spectrometer (FTS) and is capable of measuring many relevant trace gases emitted from biomass burning. Deployed on an aircraft, CU AirSOF can cover larger distances than deployed from a ground-based mobile laboratory to readily target a biomass burning event in environments that may be inaccessible by ground-based sensors, as well as pass underneath plumes spanning tens to hundreds of kilometers within a short period of time. The SOF method has been demonstrated to quantify emission fluxes using a ground-based mobile laboratory driving around agricultural[9] and industrial sources.[10−13] A suite of stationary deployed portable solar absorption FTS instruments can be used for source apportionment of greenhouse gases.[14−16] High-resolution stationary FTS affiliated with the Network for Detection of Atmospheric Composition Change (NDACC, www.ndacc.org) have detected and attributed trace gas enhancements to wildfires.[17−21] Infrared spectroscopy has good sensitivity, selectivity, is inherently calibrated (from knowledge of absorption cross sections tabulated in databases such as HITRAN), and measures a large variety of trace gases simultaneously and directly in the open atmosphere.

Previous airborne studies of biomass burning that have used FTS measured absorption using in situ techniques[22−24] and emission spectra using remote sensing techniques.[25] Airborne remote sensing FTS measurements have recorded spectra at latitudes ranging from the equator to the north pole using emission spectra,[26] derived stratospheric column amounts in Arctic winter and the polar vortex using emission spectra,[27] observed the polar vortex using both solar and emission spectra,[28] and for observations of changes in stratospheric trace gas concentrations between different latitudes such as the equator and midlatitudes by obtaining solar spectra.[28−32] To our knowledge, no airborne studies of biomass burning using solar absorption spectra have been reported. The major advantages of remote-sensing measurements using absorption rather than emission are the high photon flux and the straightforward interpretation of air mass factors. Using direct sun spectra allows for rapid data collection and excellent signal-to-noise, which in turn translates into sampling with good spatial resolution suitable in airborne applications in wildfire plumes.

Here, we describe the CU AirSOF instrument and evaluate its performance and measurements taken during the BB-FLUX (Biomass Burning Flux Measurements of Trace Gases and Aerosols) field campaign in summer 2018.[33] CU AirSOF was deployed on the University of Wyoming King Air (UWKA) research aircraft during 37 research flights (RFs) of about 2−4 h duration between 21 July and 17 September 2018. The RFs targeted isolated fires in the Pacific Northwestern U.S. with the aircraft primarily based out of Boise, Idaho. The BB-FLUX campaign's science objectives included to quantify emissions from wildfires, study plume injection height, probe photochemical ozone formation, and exploit synergies between in situ and column observations to derive speciated total emissions.[33] From the instruments operated onboard the UWKA during BB-FLUX, CU AirSOF is the primary instrument relevant to this work. CU AirSOF test flights in 2017 targeted fires in California[6] and applied similar retrieval methods as the ones evaluated in this work. A subset of BB-FLUX flights were coordinated with satellites.[34] Furthermore, the National Science Foundation/National Center for Atmospheric Research (NSF/NCAR) C-130 aircraft deployed complementary in situ instrumentation as part of the WE-CAN (Western wildfire Experiment for Cloud chemistry, Aerosol absorption, and Nitrogen) field campaign and conducted 16 RFs out of Boise, Idaho between 24 July and 28 August 2018 (https://www.eol.ucar.edu/field_projects/we-can). Here, we compare the measurements of the prototype CU AirSOF in flight with colocated in situ sensors and expand and evaluate the suite of trace gas retrievals. To further assess the accuracy of CU AirSOF, the instrument was also colocated after the BB-FLUX campaign with a high-resolution FTS (HR-FTS,[35] Supplement text) at NCAR in Boulder, Colorado.

2. CU AIRBORNE SOF INSTRUMENT

The CU AirSOF instrument builds on earlier developments as described in Kille et al.[9] and Baidar et al.[36] Several major modifications were implemented to fulfill the requirements for airborne deployment, and several modifications improve the overall performance of the system to specifically target biomass burning emissions. Only the differences between the CU AirSOF and ground-based CU mobile SOF instrument will be described here as well as the expanded data set.

The instrumental setup of CU AirSOF and the components are shown in Figure 1 and further explained in Section 2.1.

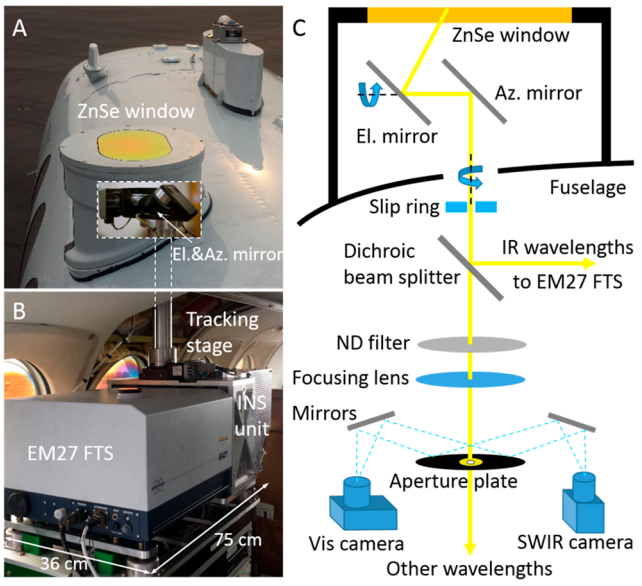

Figure 1. Instrumental setup during BB-FLUX. (A) Top view toward the nose of the UWKA showing the enclosure for the solar tracking mirrors including a ZnSe window viewport. (B) CU AirSOF mounted inside the aircraft with a long vertical tube connecting to the tracking mirrors. (C) Optical schematic of the modified digital solar tracker.

Figure 1 shows that photons along the direct solar beam enter through a zinc selenide (ZnSe) window into the aircraft and are reflected by optical components of the solar tracker to reach the FTS and solar tracking imaging system. The solar tracker itself is comprised of forward steering mirrors and a set of two cameras, one using visible light and one using SWIR (shortwave infrared) that can be switched using the software to actively track the sun.

https://doi.org/10.1021/acsearthspacechem.1c00281
ACS Earth Space Chem. 2022, 6, 582−596

2.1. Airborne Digital Solar Tracker. *2.1.1. Tracker Components.* The CU AirSOF instrument uses a custom-built digital solar tracker that has been modified from the version first described by Baidar et al.[36] for application from an aircraft platform to observe optically thick, with respect to ultraviolet-visible (UV−vis) but not infrared (IR) wavelengths, biomass burning plumes. Similar to the original solar tracker, a pair of mirrors is used to correct for platform motion with access to Euler angles (fixed coordinate system of the sun) and coarse tracking derived from an inertial navigation system (INS) that characterizes the platform's orientation. Fine tracking is provided by observing an image of the sun on an aperture plate and an imaging feedback loop utilizing a single, visible wavelength camera. The camera used for fine tracking originally described was replaced with a newer and faster high-performance model (National Instruments 1772, 480 × 640 pixels, 400−1000 nm). In anticipation of the need for solar tracking in more optically thick environments, a second camera was added (Xenics Bobcat-320, 256 × 320 pixels, 900−1700 nm), which uses longer wavelengths of light that transmit through optically thick plumes with less attenuation than the original visible wavelengths (Figure S1). The former camera is referred to as the visible camera; the latter camera is referred to as the SWIR camera. Both cameras were equipped with long-pass filters to narrow the wavelength range (900 and 1600 nm, respectively). Combined with the sensitivity range of each camera, this results in an effective 100 nm bandpass filter, 900−1000 nm and 1600−1700 nm for the visible and SWIR camera, respectively. This dual camera design allows for tracking in both clear skies and through optically thick plumes, selecting the camera with the best performance for individual situations. The choice of camera is software controlled with the visible camera as the default camera and the SWIR camera used when optical thickness along the instrument line of sight increases. The dual camera setup successfully tracked the sun under thin and thick smoke plume conditions, as well as in the absence and presence of cirrus clouds.

In addition to the changes to the cameras and software control of the instrument, structural changes were implemented to comply with airborne certification requirements. All cabling, which would cause smoke if ignited, was replaced with smokeless cabling for CU AirSOF. Additionally, the structure of the digital solar tracker was replaced with a strengthened structure designed to withstand a 9 *g* acceleration. Finally, the mount that connects the solar tracker mirrors to the camera assembly was lengthened to increase the view angles through the aircraft ZnSe window.

2.1.2. Integration on the Aircraft. The motion compensation system of the digital solar tracker was expanded from a single INS to use one of two INS inputs. This expansion was undertaken to mitigate the potential of long-term drift of a single INS system. INS systems are used with Euler angles of the sun for coarse tracking either to automatically find an initial image of the sun or when the image of the sun has been lost due to sharp aircraft motion. Motion compensation can now be performed using either the instrument internal INS (a Systron Donner Inertial MMQ-G)[36] or via the aircraft's GPS-based INS. The instrument's internal INS was operated at a data rate of 10 Hz, whereas the aircraft INS provided a data rate of 1 Hz, which is passed on to the solar tracker with an approximate 1 s delay. In general, the instrument's internal INS, which is used as the primary INS, performs better in dynamic environments such as steep turns or during turbulence due to its data rate and lack of a time lag with feedback. The aircraft INS, used as the secondary INS, performs reliably in steady flight regimes where the data rate and time lag of communication are less relevant.

Integration of the digital solar tracker on the UWKA caused vignetting with respect to direct solar viewing. When previously deployed in a mobile lab, the solar tracker mirrors could protrude from the roof hatch, allowing for near complete viewing of the sun when it was above the horizon. This is not possible given current constraints of this aircraft platform. The solar tracker mirrors were recessed slightly below an aircraft grade ZnSe window (approximate dimensions: 15 cm × 23 cm × 1 cm, long axis fore to aft) mounted on top of the UWKA fuselage. The transmission of the window in the wavelengths of interest is very near unity, but due to the recession of the mirrors the observable elevation angles are slightly restricted. This geometry remained fixed throughout deployment and is identified by knowing the physical dimensions of the window and location of the solar tracker mirrors relative to the window mount. The minimum elevation angle is a function of azimuth angle, as the orientation of the window was installed such that its long axis aligned with the aircraft fuselage. Elevation angles observable were greater than 30° for all azimuth angles, while viewing geometries near fore or aft of the aircraft allowed for observation down to approximately 20°.

2.2. Airborne EM27 FTS. The infrared spectrometer of CU AirSOF is a customized Bruker EM27 FTS. The FTS uses two detectors, indium antimonide (InSb) and mercury cadmium telluride (MCT), covering the spectral range from 700 to 5000 cm^{-1} with a resolution of 0.5 cm^{-1}. This spectral range allows a wide number of trace gases to be retrieved. The spectrometer design uses a corner cube mirror system allowing for a fast and stable acquisition during airborne application. The system hardware is the same as described by Kille et al.[9]

Operation of the spectrometer was slightly different than that described by Kille et al.[9] Typically, infrared spectra were acquired continuously at a rate of 4 scans per 1.7 s, or approximately 2.3 Hz. The sensitivity of the InSb and MCT detectors was reduced for CU AirSOF. The original sensitivity of the detectors was higher with compensation by an aperture stop to prevent permanent saturation of the detectors for CU mobile SOF. With less sensitive detector settings, the diameter of the aperture stop could be fully opened to a diameter of 2.5 cm whereas it was restricted to approximately 1 cm previously. This modification allowed CU AirSOF to compensate for larger propagation distance of the light beam between azimuthal mirror and solar tracking aperture plate, enhancing operational flexibility.

2.3. Power, Weight, and Dimensions. The CU AirSOF instrument described as installed on the UWKA research aircraft has hardware dimensions 356.0 mm width × 750.3 mm length × 788.4 mm height. Approximately half of the height is composed of an empty metal tube that spans the distance from the tracking stage to the roof of the aircraft, connecting the solar tracker mirrors to the base plate. This length is entirely dependent on the mounting specifications of the airborne platform for the instrument and can be changed as necessary. The CU AirSOF instrument in this configuration weighs approximately 38 kg. The maximum power and current observed are 483 W and 27 A. The space and weight requirement can be reduced, primarily in the vertical dimension depending on the location of the viewport.

https://doi.org/10.1021/acsearthspacechem.1c00281
ACS Earth Space Chem. 2022, 6, 582−596

Table 1. Details on the Retrieval Setup of the Target Trace Gases

species	window[a]	interfering species	a priori VCD[b]	error[c]	precision[d,e]	accuracy[d,f]	LOD[d,g]	typical VCD[h]
CO	4214−4254	H_2O, CH_4	14.	10 000	0.30	0.15	1.1	6.7
HCHO	2804−2834	H_2O, CH_4	4.5	100 000	0.23	0.28	0.97	12.
HCOOH	1096−1126	H_2O, CO_2, CH_4, O_3, NH_3, CFC-12	0.32	100 000	0.04	0.56	0.68	2.4
CH_3OH	1022−1055	H_2O, CO_2, O_3, NH_3, C_2H_4, OCS	14.	10 000	0.48	2.7[i]	4.1	10.
C_2H_4	940−980	H_2O, CO_2, O_3, NH_3, CH_3OH	0.67	100 000	0.28	0.68[i]	1.5	7.1
C_2H_6	2970−3000	H_2O, CH_4, O_3, HCHO, C_2H_4, HCl	3.9	10 000	0.14	1.1	1.5	4.9
PAN_{FTS}	775−810	H_2O, CO_2, NH_3, C_2H_2, NO_2	3.1	10 000	0.12	0.07	0.43	2.4
NH_3	940−980	H_2O, CO_2, O_3, CH_3OH, C_2H_4	2.2	10 000	0.08	0.84	1.1	9.1
HCN	3316−3351	H_2O, CO_2, N_2O, NH_3, C_2H_2	5.1	10 000	0.18	0.53	1.1	2.1

[a]In cm^{-1}. [b]In 10^{15} (10^{17} for CO) molecules cm^{-2} at 2 km msl. [c]A priori error in percent used in the retrievals. [d]In 10^{15} (10^{17} for CO) molecules cm^{-2}. [e]Calculated as the 3σ standard deviation during periods with "constant" signal (atmospheric column not changing). [f]Calculated as the mean difference between the CU AirSOF and the NCAR HR-FTS. [g]LOD calculation follows eq 2. [h]Typical in plume VCD in 10^{16} (10^{18} for CO) molecules cm^{-2}. [i]Value reflects a small non-zero offset at altitude (pristine conditions); listed only when not available from NCAR HR-FTS.

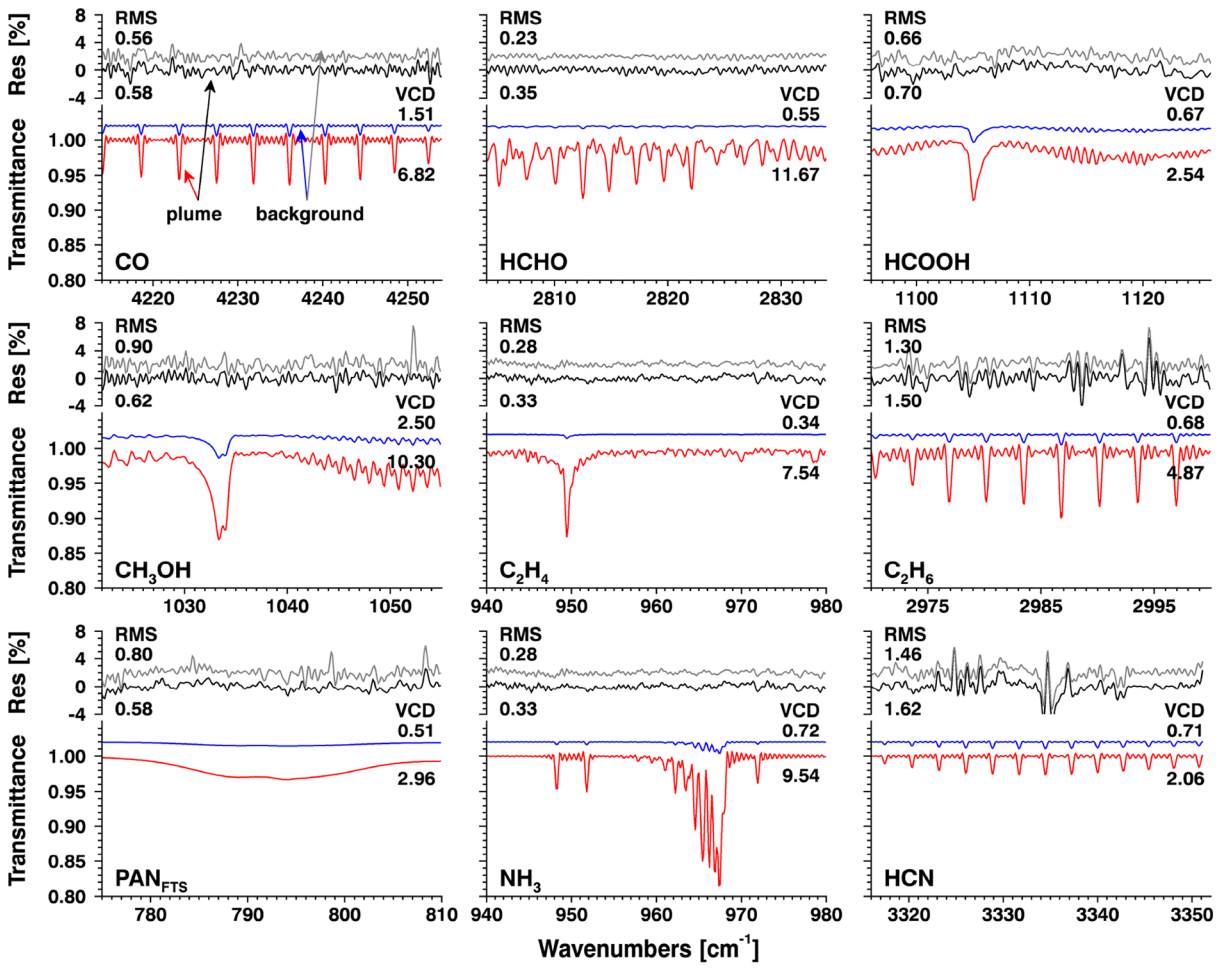

Figure 2. Spectral fits of target species for the Rabbit Foot Fire on 15 August 2018. Spectral proof of the target species showing the scaled reference spectrum (red; blue: offset by 0.02) and the residual noise between observed and calculated spectrum (black; gray: offset by 2%). The RMS is in percent, the VCD is in 10^{16} (10^{18} for CO) molecules cm^{-2}. Both plume and background spectra were acquired at about 2.1 km msl and solar zenith angle of 33°.

2.4. Trace Gas Retrievals. *2.4.1. Retrieval Windows and Spectral Proofs.* Each of the trace gases presented in this work, CO, HCHO, HCOOH, CH_3OH, C_2H_4, C_2H_6, PAN, NH_3, and HCN, is retrieved using one optimized spectral window with NH_3 and C_2H_4 being combined into a single retrieval. As the PAN cross section feature is broad and the retrieval of PAN therefore includes molecules similar to PAN, which are measured as a sum by FTS, we distinguish the PAN measured by CU AirSOF as PAN_{FTS}. Details on the retrieval setup of all gases are shown in Table 1. HCOOH, CH_3OH, C_2H_4, PAN_{FTS}, and NH_3 are retrieved at wavenumbers covered by the MCT detector, whereas CO, HCHO, C_2H_6, and HCN are retrieved in the InSb detector's spectral range. The retrievals for CU AirSOF use the SFIT4 (v0.9.4.4) retrieval software.[37] Briefly, SFIT is an optimal estimation-based retrieval algorithm, which requires a priori information on the

https://doi.org/10.1021/acsearthspacechem.1c00281
ACS Earth Space Chem. 2022, 6, 582−596

atmospheric state. The observed range of temperatures during BB-FLUX is shown in Figure S2 and accounted for in the calculation of the error budget (Section 2.4.2). The main difference in application of the retrievals for CU AirSOF compared to prior ground-based CU SOF is that the airborne deployment with fast changes in three-dimensional movement requires the dynamic dimensions of latitude, longitude, and altitude to be considered, which affect the observed solar zenith and azimuth angles. Table 1 includes the information on the interfering species that occur within the retrieval window of the target species, the a priori VCD and a priori error. A large a priori error is allowed on the target trace gas while the a priori VCD is intentionally kept lower than expected, as described by Viatte et al.[38] Precision, accuracy, and limit of detection (LOD) are described in Section 3.3 as part of the colocation analysis with a HR-FTS, which retrieves the trace gases in narrow microwindows also using SFIT4.

Spectral proofs for all trace gases measured in flight at constant altitude (~2.1 km above mean sea level (msl); 780 m above ground level (agl)) through a biomass burning plume and in background atmospheric conditions are shown in Figure 2. The residual between observed and calculated spectrum remains consistent in the presence and absence of significant trace gas enhancement. The typical column densities observed through plumes during BB-FLUX are included in Table 1 and compare to the VCDs from the observations used for the spectral proof in Figure 2.

CU AirSOF shows good vertical sensitivity across the relevant portions of the atmosphere, shown in Figure 3 for the gases of interest. Ideally the column sensitivity should be equal to 1 across all altitudes.[39] The biomass burning plumes measured during BB-FLUX resided between approximately 2 and 6 km msl. Values are calculated twice: between 2 and 6 km msl specifically for BB-FLUX and below 10 km msl to represent the troposphere. The median column sensitivity between 2 and 6 (below 10) km msl is 1.04 ± 0.03 (0.99 ± 0.04) for CO, 1.08 ± 0.02 (1.01 ± 0.10) for HCHO, 1.10 ± 0.02 (1.08 ± 0.07) for HCOOH, 0.97 ± 0.03 (0.99 ± 0.04) for CH_3OH, 1.07 ± 0.03 (1.02 ± 0.10) for C_2H_4, 1.02 ± 0.03 (1.00 ± 0.03) for C_2H_6, 1.00 ± 0.02 (1.01 ± 0.04) for PAN_{FTS}, 1.03 ± 0.01 (1.02 ± 0.04) for NH_3, and 1.03 ± 0.02 (1.01 ± 0.04) for HCN.

2.4.2. Error Budget. The total error budget of each trace gas is evaluated following the analysis method described in Viatte et al.[38] The analysis was performed on spectra taken during BB-FLUX and the colocation at NCAR post campaign with the NCAR FTS measuring at approximately 1.6 km msl and CU AirSOF observations at altitudes of the platform between approximately 1.5−2 km msl. The estimates of total error and its components are shown in Table 2 for all relevant gases and are calculated from adding random error, systematic error, and smoothing error in quadrature. Uncertainty in the measurement, temperature, retrieval parameter, interfering species, and solar zenith angle are considered random errors; uncertainty in the absorption line parameters, that is, line intensity and air-broadened half width, are considered systematic errors; the measurement error is calculated from the spectral noise and equivalent to the %RMS (root-mean-square, in percent).

Additional possible error sources could be the measurement through the ZnSe window, whose spectral transmission is not exactly unity, as well as presence of aerosol within the biomass burning plumes with absorbing properties, which are not considered in the SFIT retrievals. The specific window used during BB-FLUX has transmittance near unity. Ground-based testing performed in Boulder, Colorado prior to the airborne deployment of BB-FLUX with and without the window in place above the solar tracker mirrors did not show significant changes on the retrieved VCDs (Figure S3). Furthermore, the error caused by the absorption from aerosols was explored using CO_2, which has a large atmospheric background in the vertical column and only a relatively small enhancement due to fires. Figure S4 shows the change in CO_2 on the order of a few percent between transitions from clear background air to smoke plumes, which is well within the error. This indicates that there are no systematic effects from intensity changes caused either by absorbing aerosols or total irradiance on the detector when passing under optically thick plumes. However, spectral knowledge about the aerosol absorption refractive index is primarily limited to inorganic aerosol components,[40,41] and little is known about biomass burning aerosol absorption at IR wavelengths. There is a need for more laboratory studies on aerosol absorption properties at IR wavelengths and their inclusion into spectroscopic databases.

The findings of the total error result in the following: CO, HCOOH, C_2H_4, C_2H_6, PAN_{FTS}, and NH_3 have an uncertainty

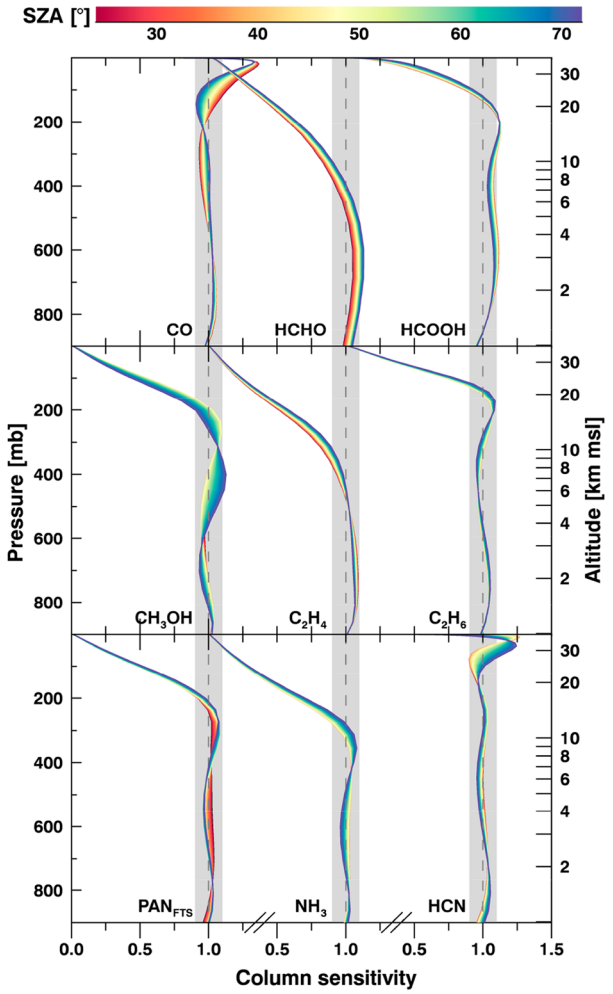

Figure 3. Column sensitivity of CO, HCHO, HCOOH, CH_3OH, C_2H_4, C_2H_6, PAN_{FTS}, NH_3, and HCN for the solar zenith angles (SZA) from 24° to 72° covered during BB-FLUX. Gray polygons represent column sensitivities within 10% of unity (dashed line).

https://doi.org/10.1021/acsearthspacechem.1c00281
ACS Earth Space Chem. 2022, 6, 582−596

Table 2. Total Error Budget and Components of Random and Systematic Uncertainties for Typical Total Columns Retrieved at Altitudes between 1.5 to 2.0 km asl

error budget (%)	CO	HCHO	HCOOH	CH_3OH	C_2H_4	C_2H_6	PAN_{FTS}	NH_3	HCN
Random									
measurement	2.3	11.	1.8	1.1	5.1	1.2	2.1	1.0	11.
temperature	1.9	2.4	2.7	1.6	4.7	3.6	1.8	2.8	9.5
retrieval parameter	4.6	20.	0.4	22.	2.5	0.6	0.0	0.4	16.
interfering species	0.4	0.3	0.1	0.1	0.4	0.1	0.2	0.1	14.
SZA	0.7	0.8	0.8	0.1	0.8	0.4	0.7	0.8	1.1
total random	5.5	23.	3.4	22.	7.4	3.9	2.9	3.1	26.
Systematic									
line intensity	1.8	9.9	4.7	6.7	5.3	2.1	9.1	1.9	10.
line width	1.9	4.1	2.8	1.7	4.8	3.7	1.8	3.0	9.8
total systematic	2.6	11.	5.4	6.9	7.1	4.2	9.3	3.6	14
Smoothing	0.6	0.7	0.1	0.1	0.0	0.5	0.3	0.2	3.9
Total error[a]	**6.1**	**26.**	**6.4**	**23.**	**10.**	**5.8**	**9.8**	**4.7**	**30.**

[a]Least square of random, systematic, and smoothing errors.

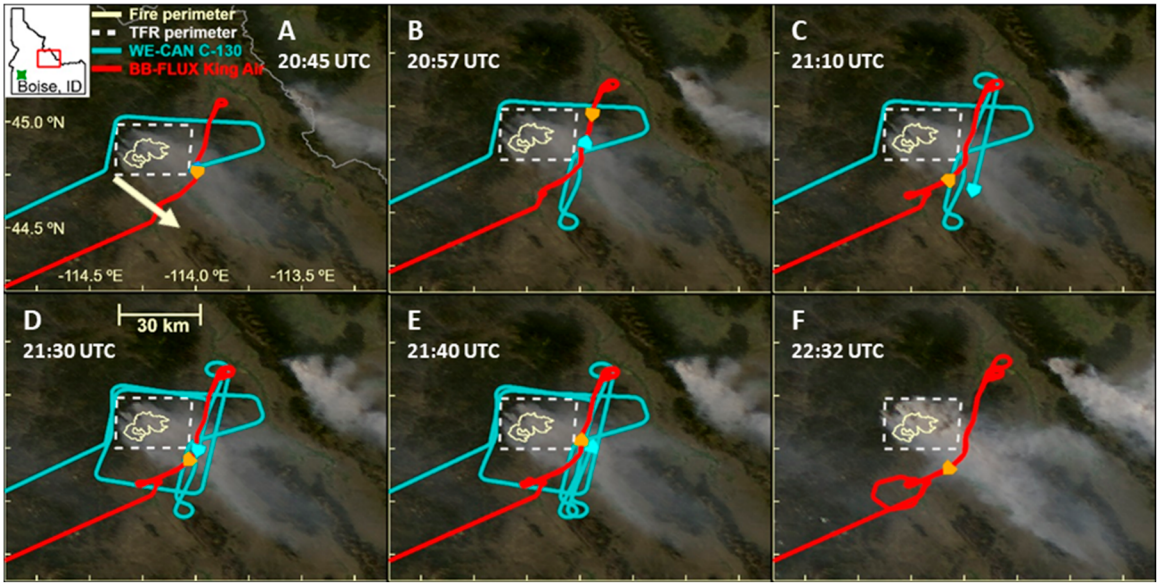

Figure 4. GOES-16 satellite image overlaid with aircraft positions and tracks, and fire perimeter within the TFR (temporary flight restriction). Panels A–F correspond to waypoints in Figure 5. The arrow indicates the wind direction and median distance covered in one hour.

of 10% or better, and HCHO, CH_3OH, and HCN have an uncertainty of 30% or better.

2.5. Performance. The performance of the solar tracker was assessed by evaluating the percent of time when the sun was successfully tracked while airborne over the duration of the BB-FLUX campaign, which was 79.6% (Table S1, Figure S5). The solar tracking success given the challenging environments and flight paths specifically flown for BB-FLUX is one major technological achievement of the CU AirSOF instrument. The causes of failed tracking were identified and grouped into mechanical and atmospheric limitations. Mechanical limitations account for 14% of the unsuccessful tracking with atmospheric limitations (excluding clouds) resulting in 3.5%. Note that these limitations were considered when flight planning so that they would have a minimum effect during plume measurements.

The first major cause of unsuccessful solar tracking was shading of the solar tracker mirrors from the window mount, occurring 6.5% of the time due to low observable elevation angles. These occurrences were mainly at the end of missions later in the day when returning from operational observations to the airport. The second major mechanical limitation was high rate-of-turn maneuvers from the aircraft in excess of the speed of the camera feedback and motor rotation rate, accounting for 6.0% of unsuccessful tracking. These errors are typically observed at the end of observational underpasses when turning around to set the aircraft up for more plume underpasses. This affects data availability but not plume measurements. Smaller mechanical limitations caused the remaining 1.5%. Atmospheric conditions, including thick clouds and strong turbulence, caused 2.5% and 1% of unsuccessful solar tracking, respectively. Other unsuccessful solar tracking is due to less significant error sources. Combined, the major atmospheric and mechanical limitations result in approximately 5% loss of the measurements desired within biomass burning plumes or required to characterize trace gas background concentrations. The remaining 15% of measurements lost can safely be discarded without loss of scientific data quality.

https://doi.org/10.1021/acsearthspacechem.1c00281
ACS Earth Space Chem. 2022, 6, 582–596

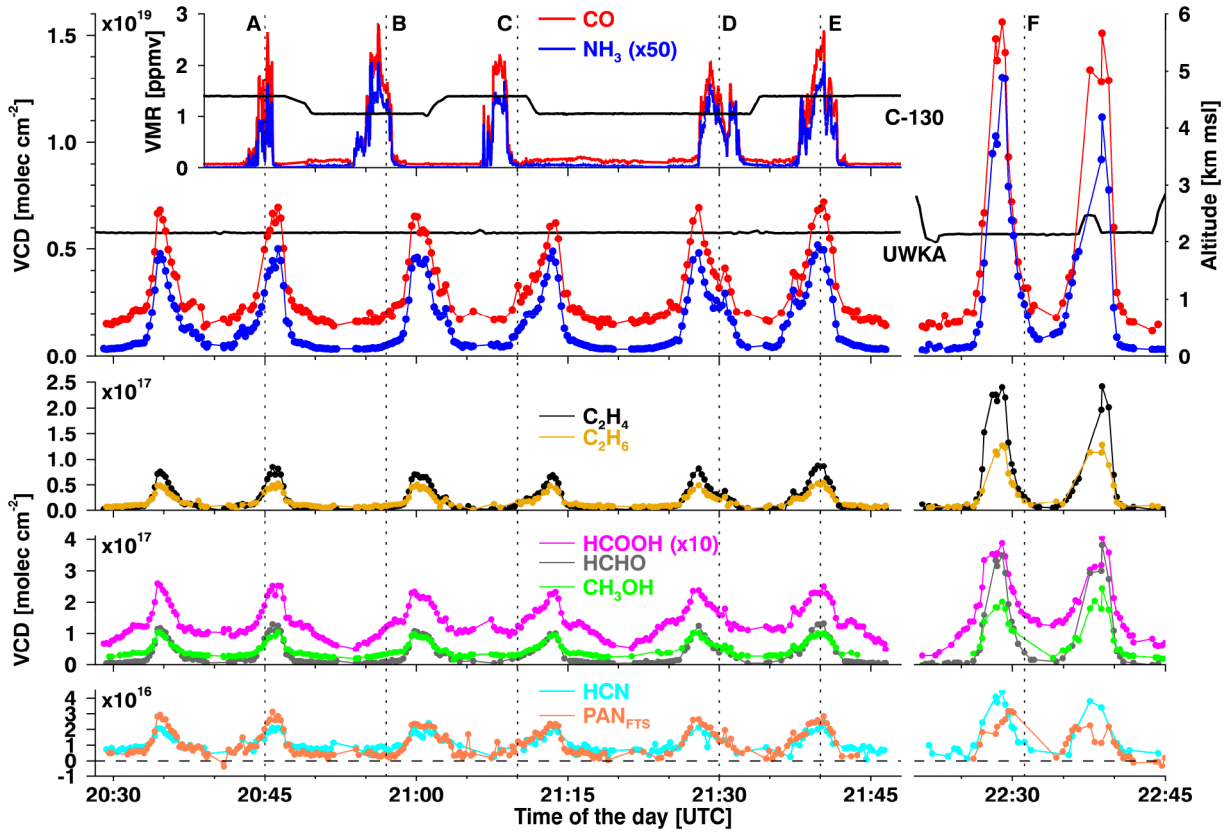

Figure 5. Timeseries of CU AirSOF VCD measurements during BB-FLUX RF13 (UWKA) targeting the Rabbit Foot Fire on 15 August 2018; the inset shows colocated in situ measurements from WE-CAN's RF11 (C-130). Aircraft altitudes are shown in black. Waypoints A−F correspond to panels in Figure 4.

Further improvements to the solar tracking performance for future deployments are most achievable by refining the mounting geometry of the solar tracker mirrors with respect to the window. Additionally, upgrading the INS to a faster and more accurate model would be expected to increase the overall success rate specifically in high rate-of-turn environments.

3. DATA SETS

3.1. Rabbit Foot Fire. An example of the measurements and capability of the CU AirSOF instrument is shown for the Rabbit Foot Fire, located at approximately 44° 52′ N, 114° 18′ W, 205 km northeast of Boise, Idaho in the Salmon-Challis National Forest. The fire was started by lightning on 2 August 2018 and burned in a biome with heavy fuel loading of subalpine fir and lodgepole pine. During BB-FLUX the UWKA sampled the fire on 8, 9, 12 (twice), and 15 August during RFs 9−13.

3.2. Coordinated Airborne Missions near Boise, Idaho. On 15 August 2018 the BB-FLUX and WE-CAN missions coordinated their research flights, sampling the Rabbit Foot Fire, to probe similar airmasses of the same smoke plume in different geometries and at different altitudes between 20:30 and 21:45 UTC (14:30−15:45 local time). Figure 4 shows a sequence of true color images from the GOES-16 satellite overlaid with the flight tracks of the two aircraft (Figure S6 shows the full BB-FLUX flight track). These images illustrate the progression of the fire activity in the later period of the flight. The wind direction remained steady at 307 ± 15° during the entire mission whereas the wind speed decreased from 9 ± 2 to 6 ± 2 m s^{-1} after 21:45 UTC. A temporary flight restriction zone (TFR), which is intended for safer firefighting operations near the burning fire, was established for the Rabbit Foot Fire and ultimately determined the nearest distance to the fire from which measurements could safely and legally be made.

3.2.1. BB-FLUX RF13. The maximum flight time of the UWKA was less than 4 h per mission for the BB-FLUX payload. RF13 was conducted from 19:41 to 23:24 UTC targeting the Rabbit Foot Fire, and CU AirSOF sampled the evolution of the fire between approximately 20:30 and 22:45 UTC. Figure 5 shows the timeseries of the different CU AirSOF measurements. BB-FLUX RF13 flew a total of eight underpasses at 2.2 km msl, or approximately 800 m agl, below the smoke plume, six of which took place during the coordinated mission with WE-CAN RF11. In order to characterize the VCD enhancement due to the smoke, level flight legs were flown, extending into atmospheric background air on either side of the smoke plume. Enhancements in all trace gases during plume underpasses are evident by local maxima in each timeseries in Figure 5. The time period between underpasses excluded from Figure 5, lasting approximately 30 min, was spent performing a vertical profile through the smoke plume for further BB-FLUX objectives focused also on the aircraft's in situ instrument payload. These data are removed here, as they are not readily comparable to underpass flight legs. The last two underpasses show much greater enhancement compared to the earlier ones, indicating

https://doi.org/10.1021/acsearthspacechem.1c00281
ACS Earth Space Chem. 2022, 6, 582−596

intensification of the fire in time, which correlates with the increase in smoke observed in the satellite images in Figure 4.

3.2.2. WE-CAN RF11. The payload of the WE-CAN campaign aboard the NSF/NCAR C-130 consisted primarily of in situ sampling instrumentation. The maximum flight time of the C-130 is approximately twice that of the UWKA. As a result, WE-CAN RF11 targeted the Rabbit Foot Fire plume for just over an hour for the mission coordination flying a total of five transects through the smoke plume prior to heading off to fulfill other WE-CAN objectives within the same flight. To measure the enhancement over background concentrations, level flight legs at both 4.5 and 4.2 km msl, approximately 3 km agl, intersected the smoke plume and extended into atmospheric background including a full loop around the TFR. Figure 5 shows the flight altitude, which is higher compared to the UWKA's due to the need to fly through the smoke and not under it, along with the in situ CO and NH_3 measurements.

WE-CAN made measurements of numerous trace gases, and the focus here is on those species that were also measured with CU AirSOF, that is, CO, HCHO, HCOOH, CH_3OH, C_2H_4, C_2H_6, PAN, NH_3, and HCN. These were measured using several different in situ techniques aboard the C-130. Here, CO measurements by an Aerodyne quantum cascade laser spectrometer (CS-108 miniQCL) are used for the analysis, which have a high precision and accuracy of 0.1 and 1 ppb, respectively. Measurements of HCHO, HCOOH, and CH_3OH are made by the proton transfer reaction time of flight mass spectrometer (PTR-ToF-MS),[42] HCHO, CH_3OH, and HCN by the trace organic gas analyzer (TOGA),[43,44] HCOOH and HCN by an iodide chemical ionization mass spectrometer (I-CIMS),[45,46] C_2H_4 and C_2H_6 by canisters collected using the advanced whole air sampler (AWAS)[47] and analyzed off-line by a five-channel gas chromatography system,[48,49] PAN by a PAN-CIMS,[50] and NH_3 by the quantum-cascade tunable infrared laser direct absorption spectrometer (TILDAS).[51]

3.2.3. Column and In Situ NEMR Calculations. A normalized excess mixing ratio (NEMR) is similar to an emission ratio (ER) but not measured directly at the source. Equation 1 defines the NEMR for trace gas X with respect to CO

$$\mathrm{NEMR}(X) = \frac{\Delta X}{\Delta \mathrm{CO}} \tag{1}$$

Here Δ denotes the difference between the in plume and out of plume measurements, in this case it is the measurement in the presence of the smoke plume and in background air, respectively. Two approaches can be considered for calculating a NEMR: the first takes the slope of the linear fit between ΔX and ΔCO, the second approach temporally integrates each of ΔX and ΔCO across the plume and then takes the ratio. On the basis of recent literature relevant to wildfires (e.g., Gilman et al.[52] or Garofalo et al.[53]) as well as discussions between both the BB-FLUX and WE-CAN science teams, the integration method was chosen for this analysis.

The calculation for column and in situ NEMR is identical with ΔX and ΔCO denoting the enhancement in the vertical column over regional background for CU AirSOF and the enhancement in volume mixing ratio over background concentrations for in situ measurements. Measurements of the different trace gases are truly colocated for CU AirSOF and have identical time resolution, as they are derived from a single spectrum from a single field of view, which allows for a straightforward NEMR calculation. In situ measurement techniques can be continuous or discrete. Among the WE-CAN observations, QCL CO, PTR-ToF-MS, I-CIMS, and TILDAS are continuous methods, whereas TOGA, AWAS, and PAN-CIMS are discrete methods such that CO was averaged to each of their sample times.

3.3. Comparison and Validation with NCAR HR-FTS in Boulder, Colorado. After the BB-FLUX field deployment of CU AirSOF, the instrument was colocated on 9 and 13 November 2018 next to the HR-FTS at NCAR in Boulder, Colorado, which is part of NDACC. CU AirSOF was positioned within 2 m of the solar tracker of the NCAR HR-FTS to observe the same air mass. CO, HCHO, HCOOH, C_2H_6, PAN_{FTS}, NH_3, and HCN VCDs were measured by the HR-FTS and compared with CU AirSOF. The data from coincident time intervals were used to determine the precision, accuracy, and LOD for the trace gases. Following the same methodology as in Kille et al.,[9] the LOD was determined using eq 2

$$\mathrm{LOD} = |\mathrm{background}| + k\cdot\sigma_{\mathrm{Gauss}} \tag{2}$$

where |background| represents the VCD in the absence of the trace gas and is determined from one or both of (I) the difference between CU AirSOF and the HR-FTS and (II) the blank measurement at high altitude from BB-FLUX. Factor k is set to 3 for a 99.7% confidence interval and σ_{Gauss} is the standard deviation during a time period in which the atmosphere remained constant.

3.4. Safety Statement. No unexpected safety hazards were encountered during the airborne sampling as well as during the ground-based measurements. Safety training was received prior to operating instrumentation aboard research aircraft and on top of the roof at NCAR.

4. RESULTS AND DISCUSSION

4.1. Ground-Based Measurements. Ground-based colocated VCD measurements from CU AirSOF and the NCAR HR-FTS taken on 9 and 13 November 2018 at NCAR in Boulder, Colorado are compared. This comparison is used to determine the LOD and accuracy of trace gases measured by both instruments (seven of the nine trace gases evaluated for CU AirSOF in this work). The HR-FTS has a spectral resolution of 0.0035 cm^{-1}, and acquisition time of approximately 205 s for CO, HCHO, C_2H_6, PAN_{FTS}, and HCN and approximately twice that duration for HCOOH and NH_3. Spectral acquisition time for CU AirSOF was variable, coadding between 4 scans (2 s) and 100 scans (38 s) per spectrum. For the comparison of the CU AirSOF measurements with those of the HR-FTS, individual data points from CU AirSOF within one HR-FTS spectral acquisition were averaged. Figure 6 shows the analyzed correlation plots of this comparison. The raw measurements are given in Figure S7 for completeness. Error bars for each system and measurement are also shown in Figure 6.

The total error is lower for the HR-FTS data compared to CU AirSOF for CO, HCHO, HCOOH, NH_3, and HCN, and approximately equal for C_2H_6 and PAN_{FTS}. All data in Figure 6, apart from the lower PAN_{FTS} observations, intercept the 1:1 line within their uncertainties. The total VCD error for CU AirSOF is expressed as the percent error caused by the cross section uncertainty and the retrieval noise at high signal-to-noise and not better than the detection limit (units of molecules cm^{-2}) at low signal-to-noise. The uncertainty for

https://doi.org/10.1021/acsearthspacechem.1c00281
ACS Earth Space Chem. 2022, 6, 582−596

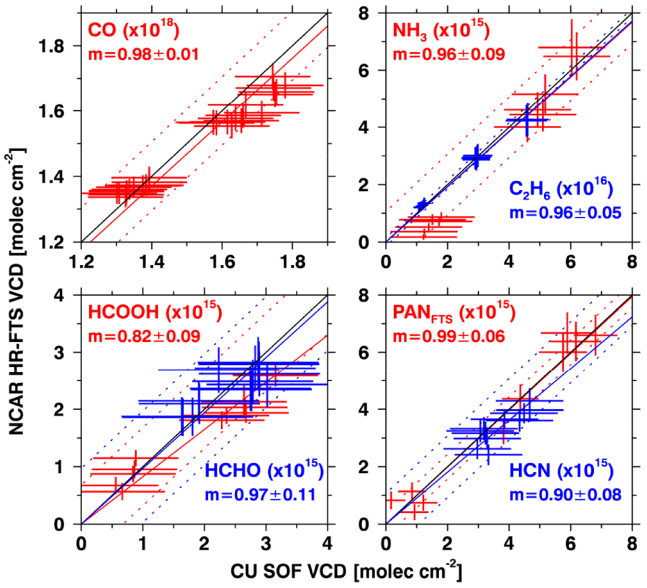

Figure 6. CU AirSOF accuracy assessment at NCAR in Boulder, Colorado on 9 and 13 November 2018. The uncertainty on the data is the total error. The solid black line represents the 1:1 line, dashed lines represent the LOD of CU AirSOF, and solid colored lines represent the fit of the bivariate orthogonal distance regression ($y = m \times x + b$ with intercept $b = 0.00$).

individual gases is 6.1% (1.1×10^{17} molecules cm^{-2}) for CO, 26.% (0.97×10^{15} molecules cm^{-2}) for HCHO, 6.4% (0.68×10^{15} molecules cm^{-2}) for HCOOH, 23.% (4.1×10^{15} molecules cm^{-2}) for CH_3OH, 10.% (1.5×10^{15} molecules cm^{-2}) for C_2H_4, 5.8% (1.5×10^{15} molecules cm^{-2}) for C_2H_6, 9.8% (0.43×10^{15} molecules cm^{-2}) for PAN_{FTS}, 4.7% (1.1×10^{15} molecules cm^{-2}) for NH_3, and 30.% (1.1×10^{15} molecules cm^{-2}) for HCN. The detection limit is calculated using eq 1, and defined using the deviation to the HR-FTS (a measure of accuracy), and the measurement precision (defined from scatter among repeat measurements). The accuracy (precision) of CU AirSOF is 0.15 (0.30) $\times 10^{17}$ for CO, 0.28 (0.23) $\times 10^{15}$ for HCHO, 0.56 (0.04) $\times 10^{15}$ for HCOOH, 2.7 (0.48) $\times 10^{15}$ for CH_3OH, 0.68 (0.28) $\times 10^{15}$ for C_2H_4, 1.1 (0.14) $\times 10^{15}$ for C_2H_6, 0.07 (0.12) $\times 10^{15}$ for PAN_{FTS}, 0.84 (0.08) $\times 10^{15}$ for NH_3, and 0.53 (0.18) $\times 10^{15}$ molecules cm^{-2} for HCN.

The determined LODs, listed in Table 1 and given as dashed lines in Figure 6, are over an order of magnitude below the typical VCD observed in a smoke plume for all trace gases. During BB-FLUX, VCDs of all trace gases were above the instrument detection limit in 97.8−100.% of the spectra measured exclusively during plume underpasses. For trace gas VCDs measured below 2.5 km msl, including both plume and background measurements, 100.% (CO), 98.7% (HCHO), 100.% (HCOOH), 100.% (CH_3OH), 89.1% (C_2H_4), 98.9% (C_2H_6), 97.2% (PAN_{FTS}), 100.% (NH_3), and 99.1% (HCN) of the measurements were above the detection limit.

The range of C_2H_6 VCDs observed at NCAR for CU AirSOF is approximately the same as during the colocated airborne measurements, but at the time of the NCAR measurements its sources are the oil and natural gas industry in the Colorado Front Range instead of wildfires. There is generally good agreement. The range of PAN_{FTS} VCDs observed at NCAR are a factor of 3 or 4 lower than inside the plume observed during BB-FLUX. The mid-to-high VCDs at NCAR agree well between CU AirSOF and the HR-FTS. That the CU AirSOF PAN_{FTS} NEMRs appear high in comparison to the in situ derived PAN NEMR is not expected to be the result from a bias but rather due to additional compounds contributing to PAN_{FTS} (compare Section 4.2.1).

4.2. Airborne Measurements. *4.2.1. NEMR Comparison.* NEMRs at approximately 20 km downwind of the Rabbit Foot Fire are compared for CU AirSOF remote sensing and various in situ measurements. Auxiliary measurements of wind speed and direction, latitude, longitude, and altitude from both BB-FLUX and WE-CAN were used to determine the approximate physical plume age as 0.5−1.5 h. In Figure 7, the NEMRs for the compounds detected in the individual smoke samples are reported for both the CU AirSOF and individual instruments

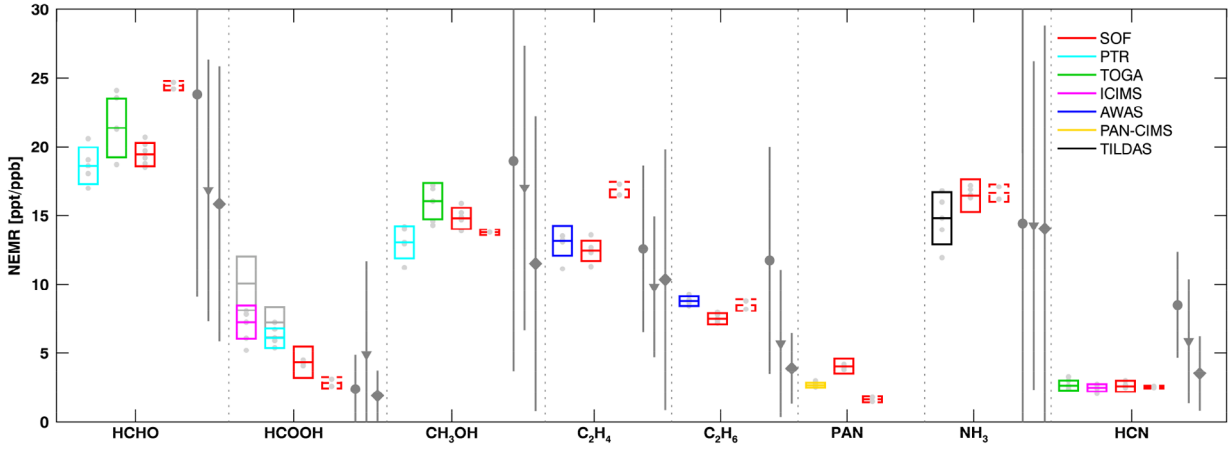

Figure 7. Comparisons of NEMRs between CU AirSOF and in situ measurement techniques for the Rabbit Foot Fire with physical plume age between 0.5 and 1.5 h. Individual NEMRs are shown as light gray filled circles, boxes show the median and standard deviation. For CU AirSOF, boxes show the median and the larger value of standard deviation and error due to choice of background (compare to Table S2). Literature values for biomass burning measurements of temperate forest are shown in gray (circle, Akagi et al.;[1] triangle, Andreae;[62] diamond, Prichard et al.[63]). Note that these values are ERs since they are for fresh, unprocessed emissions whereas the observations are for plume ages between 0.5 and 1.5 h. The dashed CU AirSOF NEMRs correspond to the latter two underpasses from Figure 5 after 22:00 UTC. The gray in situ HCOOH NEMRs are calculated using the standard background selection.

https://doi.org/10.1021/acsearthspacechem.1c00281
ACS Earth Space Chem. 2022, 6, 582−596

from WE-CAN. Additionally, a selection of literature values commonly used by emission inventories are shown for comparison.

Figure 7 shows comparisons of NEMR data for overlapping species measured aboard both aircraft during the colocated underpasses. Additionally, Figure 7 includes NEMR data from two additional underpasses from the CU AirSOF instrument taken in aged smoke after the C-130 left the Rabbit Foot Fire. Each measured NEMR is given as a single dot, and whisker boxes indicate the median and 1σ standard deviation (or error due to background subtraction, whichever is larger). As can be seen in Figure 5, the background VCDs on either side of the smoke plume are not necessarily identical, as is particularly clear for HCOOH. Therefore, in order to evaluate the agreement between the column and in situ measured NEMRs the standard deviation among the individual NEMRs and the influence of variable background need to be considered.

CU AirSOF median NEMRs agree for most species to better than 20% (see Figure 7, and Table S2) with the in situ measurement derived median NEMRs. Agreement within standard deviation is found for NEMRs of HCHO (PTR-ToF-MS and TOGA), C_2H_4 (AWAS), NH_3 (TILDAS), CH_3OH (PTR-ToF-MS and TOGA), and HCN (TOGA and I-CIMS). Agreement within the NEMR uncertainty is found for the NEMRs of C_2H_6 (AWAS).

For PAN, the median column NEMR for PAN_{FTS} is systematically larger than measured by PAN-CIMS by about 50%. This is attributed to the fact that CU AirSOF measures selected acyl peroxy nitrates (APNs) as a sum, including PAN and other PAN-like compounds (e.g., peroxy propionylnitrate (PPN), peroxy alkyl nitrates (PAkNs)) that exhibit a similar absorption spectrum near 794 cm^{-1}[54,55]; notably PAN derived from acrolein (APAN), or crotonaldehyde (CPAN) do not contribute significant absorption in this spectral region.[56] Since PAN typically comprises about 80% of the total speciated APNs,[57,58] the contribution from PPN and possibly other APNs that add to the PAN absorption near 794 cm^{-1} is likely on the order of 10%. PAN-CIMS derived PPN to PAN ratios during WE-CAN of fresh plumes (1−6 h) averaged 12%,[59] and a similar PPN to PAN ratio of 11% was observed for a Siberian biomass burning plume.[60] An overview of APNs measured at Mount Bachelor, Oregon is given by Wolfe et al.[61] and indicates that when PPN to PAN is 10% then MPAN (peroxymethacryloyl nitrate) is 4%, APAN is 2%, and the sum of PBNs (peroxy butyryl nitrates) is 2%. A more detailed analysis of the species that contribute to the PAN_{FTS} signal remains desirable.

For HCOOH, the median NEMRs from CU AirSOF tend to be slightly lower than the NEMR from PTR-ToF-MS and I-CIMS (initially, by up to a factor of 2). HCOOH is somewhat different from the other species in that concentrations are elevated and found to be variable by in situ techniques in the boundary layer background next to the plume. While for CU AirSOF the background VCD is variable (see above discussion, and Figure 5), this variability is reduced due to the vertically integrating measurement over boundary layer height, and small compared to the variability seen by in situ sensors. The in situ NEMR of HCOOH was calculated using two methods of selecting the out-of-plume background mixing ratio. For all other gases, a standard background selection was applied (15−30 s on both sides of the plume). For direct comparison with Permar et al.,[42] the HCOOH NEMR also was calculated using the standard background selection (gray boxes for HCOOH in Figure 7). However, closer inspection of this particular plume required a more nuanced assessment of HCOOH background measurements. While the Rabbit Foot Fire plume was contained within the boundary layer, the C-130 flight track transitioned from boundary layer air to free tropospheric air on one or both sides of several of the plume transects. In the boundary layer, HCOOH backgrounds varied between approximately 5−8 ppbv, while the free troposphere contained close to 0 ppbv. The dominant source of dilution of the plume was likely from boundary layer air, so the NEMR of HCOOH was also calculated using only boundary layer backgrounds, removing any free tropospheric air from the calculation (colored boxes for HCOOH in Figure 7). This background sampling artifact may have occurred during other plumes sampled during WE-CAN, indicating the NEMR of HCOOH presented in Permar et al.[42] is likely an upper limit.

This issue will also affect in situ NEMR calculations for other compounds that have significant variability between boundary layer and free tropospheric mixing ratios. Even with the new calculation, HCOOH from both I-CIMS and PTR-ToF-MS are 40−66% higher than the NEMR measured by CU AirSOF, and are also higher than previous laboratory and synthesis studies. The reasons for this apparent discrepancy is currently unclear. The calibration uncertainty of the I-CIMS and PTR-ToF-MS is ∼30% and is only marginally sufficient to explain the observed differences. It therefore appears that other contributing factors arise from real differences between in situ mixing ratios near the plume top (where photochemical production may be relatively enhanced) compared with the average of the column measurement and added uncertainties in background subtraction caused by vertical HCOOH gradients in the air with which the plume diluted as it rose. A systematic comparison of CIMS/PTR-ToF-MS calibrations with spectroscopic standards is desirable, and holds potential to investigate questions about vertical gradients in HCOOH NEMRs inside wildfire plumes further in the future.

The CU AirSOF VCDs measured after the C-130 departed have generally much larger enhancements and the NEMRs show variability compared to the earlier values (time-resolved values are listed in Table S3). An increase in NEMR is observed for HCHO, C_2H_4, and C_2H_6. NEMRs decreased for HCOOH, CH_3OH, and PAN_{FTS}. No change could be determined for NH_3 and HCN. During the later period after the C-130 left the vicinity is characterized by decreased wind speeds, thicker smoke, and reduced radiation inside the plume.

4.2.2. Comparison with Literature Values. Figure 7 includes NEMRs calculated using the emission factors averages (EFs) compiled in Akagi et al.,[1] Andreae,[62] and Prichard et al.[63] for the temperate forest category, a vegetation type prevalent in the Rabbit Foot Fire. The EFs encompass field and lab measurements from separate fires with comparable age and vegetation type. The EFs were converted to NEMRs (ppt ppb^{-1}) by dividing the EF of the chemical species of interest by the CO EF and accounting for their molar masses. NEMRs values are shown as solid gray markers indicating the mean and an error bar denoting the standard deviation. Relatively large spreads in the literature-derived NEMRs are observed for all chemical species, reflecting a significant variability in fire behavior.[1] Differences in mean values are also observed, which may be due to the different averaging methods considered in the EFs compilation.[1] WE-CAN observations found that agreement between EFs is better when only comparing across

https://doi.org/10.1021/acsearthspacechem.1c00281
ACS Earth Space Chem. 2022, 6, 582−596

similar fire behaviors.[64] In particular, Akagi et al.[1] display larger mean values than Andreae[62] and Prichard et al.[63] for most chemical species except for HCOOH. The mean values on Prichard et al.,[63] on the other hand, tend to be lower than the rest of the studies, except for C_2H_4, with the mean being a value emission inventories might use.

For most chemical species, the literature-derived values are aligned with the CU AirSOF NEMRs (red boxes). CU AirSOF median values are generally larger than the literature-derived mean values for HCHO, HCOOH, C_2H_4, C_2H_6, and NH_3. Up to 30% for HCHO, C_2H_4, and NH_3, and as much as 132% for HCOOH (e.g., Prichard et al.[63]). C_2H_6 NEMRs can be up to 92% higher than most literature ones, except for Akagi et al., where values can be up to 36% lower.

While our values are larger for most of the species discussed above, for HCN, the CU AirSOF NEMR was found to be lower than the derived literature values (up to 69% lower, e.g., Akagi et al.[1]). For CH_3OH, the CU AirSOF measurements are on the lower end of the range reported in the literature by up to 22%, except for Prichard et al.,[63] where values can be up to 29% higher. The underlying data are included in Table S2. In summary, the agreement with mean literature values is within a factor of 2 with the exception of HCN where Akagi et al.[1] is within a factor of 3; a factor of 2 is considered good agreement when comparing those obtained in the lab with field measurements.[65]

5. CONCLUSION AND OUTLOOK

We conclude that adding the ability to track the sun with SWIR wavelengths enhances CU AirSOF observations in optically thick wildfire plumes. CU AirSOF measurements provide high quality trace gas VCD measurements of a large variety of gases. CU AirSOF performs unique measurements on extended spatial scales also in complex terrain, where a ground-based mobile laboratory would not have access.

The comparison of CU AirSOF observations with external information is summarized as follows:

- The colocated stationary ground-based measurements with HR-FTS are well correlated with slopes ranging from 0.82 ± 0.09 to 0.99 ± 0.06. The HR-FTS does not evaluate CH_3OH and C_2H_4.
- CU AirSOF derived NEMRs for all nine trace gases are compared to in situ NEMRs from six instruments during the sampling of a wildfire plume. Direct comparisons show agreement within 12% for HCHO (PTR-ToF-MS and TOGA), CH_3OH (PTR-ToF-MS and TOGA), C_2H_4 (AWAS), NH_3 (TILDAS), and HCN (TOGA and I-CIMS) and within 35% for C_2H_6 (AWAS) and PAN (PAN-CIMS). HCOOH (compared to I-CIMS and PTR-ToF-MS) shows better agreement (40−66%) when a boundary layer background was chosen instead of standard background subtraction (NEMR from I-CIMS a factor 2 greater than from CU AirSOF).
- The reasons for this discrepancy in the in situ HCOOH NEMR warrant further investigation. A more detailed analysis of the APN speciation to assess minor contributions from species other than PAN in PAN_{FTS} signals remains desirable.

The comparison of NEMR with those based on literature values representative of atmospheric emission inventories is summarized as follows:

- Emission inventories distinguish between different biomes such as savanna, temperate forest, and extratropical forest and possibly also between flaming and smoldering state of a fire. The Rabbit Foot Fire is compared to the temperate forest category. There is spread around the mean reported values of up to a factor of 2.4 (e.g., Akagi et al.[1] and Prichard et al.[63] for NH_3 or Andreae[62] for HCOOH).
- Comparisons show agreement for both CU AirSOF and airborne in situ measurements within the spread around the literature means for HCHO, CH_3OH, C_2H_4, and NH_3. The HCOOH NEMRs from CU AirSOF are in good agreement with literature values. C_2H_6 agrees with Akagi et al.[1] and Andreae,[62] but Prichard et al.[63] is slightly smaller. For HCN the NEMRs fall on the lower end of Andreae[62] and Prichard et al.[63] There is no comparison for PAN as it is grouped together with other VOCs.
- We observed temporal evolution in the fire activity during the extended CU AirSOF sampling after departure of the NSF/NCAR C-130. The wind speeds decreased from 9 ± 2 to 6 ± 2 m s^{-1} without change in wind direction, which resulted in a significant increase in the CU AirSOF NEMR of primary species, and a decrease in the NEMR of secondary species.

This work described and evaluated CU AirSOF as a new tool that enables measuring emissions from distributed sources as well as the evolution of emissions in time. The SOF technique is a powerful tool to derive trace gas mass fluxes from different sources, and the ability to deploy CU AirSOF on airborne platforms in addition to ground vehicles advances the technique to conduct measurements of large or remote sources such as wildfires. Ongoing work leveraging CU AirSOF observations is being performed on a broader range of case studies from the 2017 and 2018 fire seasons.[6,33] These include studies comparing measured emission flux estimates to modeled output and a broader range of case studies encompassing more varied fire types including fuel type, fuel load, and location/topography.

■ ASSOCIATED CONTENT

Supporting Information

The Supporting Information is available free of charge at https://pubs.acs.org/doi/10.1021/acsearthspacechem.1c00281.

Additional figures and tables (PDF)

■ AUTHOR INFORMATION

Corresponding Author

Rainer Volkamer − *Department of Chemistry, Cooperative Institute for Research in Environmental Sciences, and Department of Atmospheric and Oceanic Sciences, University of Colorado Boulder, Boulder, Colorado 80309, United States;* orcid.org/0000-0002-0899-1369; Email: rainer.volkamer@colorado.edu

Authors

Natalie Kille − *Department of Chemistry, Cooperative Institute for Research in Environmental Sciences, and Department of Atmospheric and Oceanic Sciences, University of Colorado Boulder, Boulder, Colorado 80309, United States;* Present Address: Institute of Energy and Climate

https://doi.org/10.1021/acsearthspacechem.1c00281
ACS Earth Space Chem. 2022, 6, 582−596

Research: Troposphere (IEK-8), Forschungszentrum Jülich GmbH, 52425 Jülich, Germany; orcid.org/0000-0001-7116-8132
Kyle J. Zarzana − *Department of Chemistry, University of Colorado Boulder, Boulder, Colorado 80309, United States;* orcid.org/0000-0003-1581-6419
Johana Romero Alvarez − *Department of Chemistry, University of Colorado Boulder, Boulder, Colorado 80309, United States*
Christopher F. Lee − *Department of Chemistry and Cooperative Institute for Research in Environmental Sciences, University of Colorado Boulder, Boulder, Colorado 80309, United States*
Jake P. Rowe − *Department of Chemistry and Cooperative Institute for Research in Environmental Sciences, University of Colorado Boulder, Boulder, Colorado 80309, United States*
Benjamin Howard − *Department of Chemistry, University of Colorado Boulder, Boulder, Colorado 80309, United States*
Teresa Campos − *Atmospheric Chemistry Observations and Modeling, National Center for Atmospheric Research, Boulder, Colorado 80301, United States*
Alan Hills − *Atmospheric Chemistry Observations and Modeling, National Center for Atmospheric Research, Boulder, Colorado 80301, United States*
Rebecca S. Hornbrook − *Atmospheric Chemistry Observations and Modeling, National Center for Atmospheric Research, Boulder, Colorado 80301, United States;* orcid.org/0000-0002-6304-6554
Ivan Ortega − *Atmospheric Chemistry Observations and Modeling, National Center for Atmospheric Research, Boulder, Colorado 80301, United States*
Wade Permar − *Department of Chemistry and Biochemistry, University of Montana, Missoula, Montana 59812, United States*
I Ting Ku − *Department of Atmospheric Science, Colorado State University, Fort Collins, Colorado 80521, United States*
Jakob Lindaas − *Department of Atmospheric Science, Colorado State University, Fort Collins, Colorado 80521, United States*
Ilana B. Pollack − *Department of Atmospheric Science, Colorado State University, Fort Collins, Colorado 80521, United States;* orcid.org/0000-0001-7151-9756
Amy P. Sullivan − *Department of Atmospheric Science, Colorado State University, Fort Collins, Colorado 80521, United States*
Yong Zhou − *Department of Atmospheric Science, Colorado State University, Fort Collins, Colorado 80521, United States*
Carley D. Fredrickson − *Department of Atmospheric Sciences, University of Washington, Seattle, Washington 98195, United States*
Brett B. Palm − *Department of Atmospheric Sciences, University of Washington, Seattle, Washington 98195, United States;* Present Address: Atmospheric Chemistry Observations and Modeling, National Center for Atmospheric Research, Boulder, Colorado 80301, U.S.A.
Qiaoyun Peng − *Department of Atmospheric Sciences, University of Washington, Seattle, Washington 98195, United States*
Eric C. Apel − *Atmospheric Chemistry Observations and Modeling, National Center for Atmospheric Research, Boulder, Colorado 80301, United States*
Lu Hu − *Department of Chemistry and Biochemistry, University of Montana, Missoula, Montana 59812, United States*
Jeffrey L. Collett, Jr. − *Department of Atmospheric Science, Colorado State University, Fort Collins, Colorado 80521, United States*
Emily V. Fischer − *Department of Atmospheric Science, Colorado State University, Fort Collins, Colorado 80521, United States*
Frank Flocke − *Atmospheric Chemistry Observations and Modeling, National Center for Atmospheric Research, Boulder, Colorado 80301, United States*
James W. Hannigan − *Atmospheric Chemistry Observations and Modeling, National Center for Atmospheric Research, Boulder, Colorado 80301, United States*
Joel Thornton − *Department of Atmospheric Sciences, University of Washington, Seattle, Washington 98195, United States;* orcid.org/0000-0002-5098-4867

Complete contact information is available at: https://pubs.acs.org/10.1021/acsearthspacechem.1c00281

Author Contributions

R.V. designed the research. N.K., K.J.Z., C.F.L., B.H., and R.V. performed field measurements. T.C., A.H., R.S.H., L.H., I.T.K., J.L., W.P., I.B.P., A.P.S., Y.Z., B.B.P., Q.P., C.D.F., E.C.A., J.L.C., E.V.F., F.F., and J.T. contributed aircraft data, I.O. and J.W.H. contributed ground-based data. N.K., K.J.Z., J.R., C.F.L., J.P.R., W.P., and B.B.P. analyzed data. N.K. and R.V. wrote the paper with contributions from all coauthors.

Notes

The authors declare no competing financial interest.
The BB-FLUX dataset is available from https://data.eol.ucar.edu/project/BB-FLUX. WE-CAN data are available from https://data.eol.ucar.edu/master_lists/generated/we-can/ (Merge version R4 is used in this study).

■ ACKNOWLEDGMENTS

Financial support for the BB-FLUX project is from National Science Foundation (NSF) Grant AGS-1754019. This material is based upon work supported by the National Center for Atmospheric Research (NCAR), which is a major facility sponsored by the National Science Foundation under Cooperative Agreement No. 1852977. The NCAR FTS observation program at Boulder, Colorado is supported by the National Aeronautics and Space Administration (NASA). WE-CAN data were collected using NSF's Lower Atmosphere Observing Facilities, which are managed and operated by NCAR's Earth Observing Laboratory. I.T.K., J.L., I.B.P., A.P.S, J.L.C., and E.V.F. were supported by NSF Grant AGS-1650786. W.P. and L.H. were supported by NSF Grant AGS-1650275. B.B.P., Q.P., C.D.F., and J.T. were supported by NSF Grant AGS-1652688 and National Oceanic and Atmospheric Administration (NOAA) Grant NA17OAR4310012. C.F.L. received summer support from the Department of Chemistry at CU Boulder. We thank David Thomson for software development and support during system integration on the aircraft. We thank Dr. Theodore Koenig for useful discussions. We thank the entire BB-FLUX and WE-CAN science teams, the pilots of both aircraft, and the entire UW Flight Center staff.

REFERENCES

(1) Akagi, S. K.; Yokelson, R. J.; Wiedinmyer, C.; Alvarado, M. J.; Reid, J. S.; Karl, T.; Crounse, J. D.; Wennberg, P. O. Emission Factors for Open and Domestic Biomass Burning for Use in Atmospheric Models. *Atmospheric Chemistry and Physics* **2011**, *11* (9), 4039−4072.

(2) Crutzen, P. J.; Andreae, M. O. Biomass Burning in the Tropics: Impact on Atmospheric Chemistry and Biogeochemical Cycles. *Science* **1990**, *250* (4988), 1669−1678.

(3) Chen, J.; Li, C.; Ristovski, Z.; Milic, A.; Gu, Y.; Islam, M. S.; Wang, S.; Hao, J.; Zhang, H.; He, C.; Guo, H.; Fu, H.; Miljevic, B.; Morawska, L.; Thai, P.; LAM, Y. F.; Pereira, G.; Ding, A.; Huang, X.; Dumka, U. C. A Review of Biomass Burning: Emissions and Impacts on Air Quality, Health and Climate in China. *Science of The Total Environment* **2017**, *579*, 1000−1034.

(4) Reid, C. E.; Brauer, M.; Johnston, F. H.; Jerrett, M.; Balmes, J. R.; Elliott, C. T. Critical Review of Health Impacts of Wildfire Smoke Exposure. *Environ. Health Perspect.* **2016**, *124* (9), 1334−1343.

(5) Carter, T. S.; Heald, C. L.; Jimenez, J. L.; Campuzano-Jost, P.; Kondo, Y.; Moteki, N.; Schwarz, J. P.; Wiedinmyer, C.; Darmenov, A. S.; Da Silva, A. M.; Kaiser, J. W. How Emissions Uncertainty Influences the Distribution and Radiative Impacts of Smoke from Fires in North America. *Atmospheric Chemistry and Physics* **2020**, *20* (4), 2073−2097.

(6) Bela, M. M.; Kille, N.; McKeen, S. A.; Romero-Alvarez, J.; Ahmadov, R.; James, E.; Pereira, G.; Schmidt, C.; Pierce, R. B.; O'Neill, S. M.; Zhang, X.; Kondragunta, S.; Wiedinmyer, C.; Volkamer, R. Quantifying Carbon Monoxide Emissions on the Scale of Large Wildfires. *Geophys. Res. Lett.* **2022**, DOI: 10.1029/2021GL095831.

(7) National Academies of Sciences, Engineering, and Medicine. The Future of Atmospheric Chemistry Research: Remembering Yesterday, Understanding Today, Anticipating Tomorrow. *Future of Atmospheric Chemistry Research* **2016**, DOI: 10.17226/23573.

(8) Val Martin, M.; Logan, J. A.; Kahn, R. A.; Leung, F. Y.; Nelson, D. L.; Diner, D. J. Smoke Injection Heights from Fires in North America: Analysis of 5 Years of Satellite Observations. *Atmospheric Chemistry and Physics* **2010**, *10* (4), 1491−1510.

(9) Kille, N.; Baidar, S.; Handley, P.; Ortega, I.; Sinreich, R.; Cooper, O. R.; Hase, F.; Hannigan, J. W.; Pfister, G.; Volkamer, R. The CU Mobile Solar Occultation Flux Instrument: Structure Functions and Emission Rates of NH3, NO2 and C2H6. *Atmospheric Measurement Techniques* **2017**, *10* (1), 373−392.

(10) Johansson, J. K. E.; Mellqvist, J.; Samuelsson, J.; Offerle, B.; Moldanova, J.; Rappenglück, B.; Lefer, B.; Flynn, J. Quantitative Measurements and Modeling of Industrial Formaldehyde Emissions in the Greater Houston Area during Campaigns in 2009 and 2011. *Journal of Geophysical Research: Atmospheres* **2014**, *119* (7), 4303−4322.

(11) Johansson, J. K. E.; Mellqvist, J.; Samuelsson, J.; Offerle, B.; Lefer, B.; Rappenglück, B.; Flynn, J.; Yarwood, G. Emission Measurements of Alkenes, Alkanes, SO2, and NO2 from Stationary Sources in Southeast Texas over a 5 Year Period Using SOF and Mobile DOAS. *Journal of Geophysical Research: Atmospheres* **2014**, *119* (4), 1973−1991.

(12) Mellqvist, J.; Samuelsson, J.; Johansson, J.; Rivera, C.; Lefer, B.; Alvarez, S.; Jolly, J. Measurements of Industrial Emissions of Alkenes in Texas Using the Solar Occultation Flux Method. *Journal of Geophysical Research: Atmospheres* **2010**, *115* (D7), 0−17.

(13) Samuelsson, J.; Delre, A.; Tumlin, S.; Hadi, S.; Offerle, B.; Scheutz, C. Optical Technologies Applied alongside On-Site and Remote Approaches for Climate Gas Emission Quantification at a Wastewater Treatment Plant. *Water Res.* **2018**, *131*, 299−309.

(14) Jones, T.; Franklin, J.; Chen, J.; Dietrich, F.; Hajny, K.; Paetzold, J.; Wenzel, A.; Gately, C.; Gottlieb, E.; Parker, H.; Dubey, M.; Hase, F.; Shepson, P.; Mielke, L.; Wofsy, S. Assessing Urban Methane Emissions Using Column Observing Portable FTIR Spectrometers and a Novel Bayesian Inversion Framework. *Atmospheric Chemistry and Physics* **2021**, *21*, 13131.

(15) Kille, N.; Chiu, R.; Frey, M.; Hase, F.; Sha, M. K.; Blumenstock, T.; Hannigan, J. W.; Orphal, J.; Bon, D.; Volkamer, R. Separation of Methane Emissions From Agricultural and Natural Gas Sources in the Colorado Front Range. *Geophys. Res. Lett.* **2019**, *46* (7), 3990−3998.

(16) Viatte, C.; Lauvaux, T.; Hedelius, J. K.; Parker, H.; Chen, J.; Jones, T.; Franklin, J. E.; Deng, A. J.; Gaudet, B.; Verhulst, K.; Duren, R.; Wunch, D.; Roehl, C.; Dubey, M. K.; Wofsy, S.; Wennberg, P. O. Methane Emissions from Dairies in the Los Angeles Basin. *Atmospheric Chemistry and Physics* **2017**, *17* (12), 7509−7528.

(17) Paton-Walsh, C.; Jones, N. B.; Wilson, S. R.; Haverd, V.; Meier, A.; Griffith, D. W. T.; Rinsland, C. P. Measurements of Trace Gas Emissions from Australian Forest Fires and Correlations with Coincident Measurements of Aerosol Optical Depth. *Journal of Geophysical Research: Atmospheres* **2005**, *110* (D24), 1−6.

(18) Viatte, C.; Strong, K.; Hannigan, J.; Nussbaumer, E.; Emmons, L. K.; Conway, S.; Paton-Walsh, C.; Hartley, J.; Benmergui, J.; Lin, J. Identifying Fire Plumes in the Arctic with Tropospheric FTIR Measurements and Transport Models. *Atmospheric Chemistry and Physics* **2015**, *15* (5), 2227−2246.

(19) Lutsch, E.; Dammers, E.; Conway, S.; Strong, K. Long-Range Transport of NH3, CO, HCN, and C2H6 from the 2014 Canadian Wildfires. *Geophys. Res. Lett.* **2016**, *43* (15), 8286−8297.

(20) Lutsch, E.; Strong, K.; Jones, D. B. A.; Ortega, I.; Hannigan, J. W.; Dammers, E.; Shephard, M. W.; Morris, E.; Murphy, K.; Evans, M. J.; Parrington, M.; Whitburn, S.; Van Damme, M.; Clarisse, L.; Coheur, P.-F.; Clerbaux, C.; Croft, B.; Martin, R. V.; Pierce, J. R.; Fisher, J. A. Unprecedented Atmospheric Ammonia Concentrations Detected in the High Arctic From the 2017 Canadian Wildfires. *Journal of Geophysical Research: Atmospheres* **2019**, *124* (14), 8178−8202.

(21) Lutsch, E.; Strong, K.; Jones, D. B. A.; Blumenstock, T.; Conway, S.; Fisher, J. A.; Hannigan, J. W.; Hase, F.; Kasai, Y.; Mahieu, E.; Makarova, M.; Morino, I.; Nagahama, T.; Notholt, J.; Ortega, I.; Palm, M.; Poberovskii, A. V.; Sussmann, R.; Warneke, T. Detection and Attribution of Wildfire Pollution in the Arctic and Northern Midlatitudes Using a Network of Fourier-Transform Infrared Spectrometers and GEOS-Chem. *Atmospheric Chemistry and Physics* **2020**, *20* (21), 12813−12851.

(22) Yokelson, R. J.; Goode, J. G.; Ward, D. E.; Susott, R. A.; Babbitt, R. E.; Wade, D. D.; Bertschi, I.; Griffith, D. W. T.; Hao, W. M. Emissions of Formaldehyde, Acetic Acid, Methanol, and Other Trace Gases from Biomass Fires in North Carolina Measured by Airborne Fourier Transform Infrared Spectroscopy. *Journal of Geophysical Research: Atmospheres* **1999**, *104* (D23), 30109−30125.

(23) Goode, J. G.; Yokelson, R. J.; Ward, D. E.; Susott, R. A.; Babbitt, R. E.; Davies, M. A.; Hao, W. M. Measurements of Excess O3, CO2, CO, CH4, C2H4, C2H2, HCN, NO, NH3, HCOOH, CH3COOH, HCHO, and CH3OH in 1997 Alaskan Biomass Burning Plumes by Airborne Fourier Transform Infrared Spectroscopy (AFTIR). *Journal of Geophysical Research: Atmospheres* **2000**, *105* (D17), 22147−22166.

(24) Burling, I. R.; Yokelson, R. J.; Akagi, S. K.; Urbanski, S. P.; Wold, C. E.; Griffith, D. W. T.; Johnson, T. J.; Reardon, J.; Weise, D. R. Airborne and Ground-Based Measurements of the Trace Gases and Particles Emitted by Prescribed Fires in the United States. *Atmospheric Chemistry and Physics* **2011**, *11* (23), 12197−12216.

(25) Worden, H.; Beer, R.; Rinsland, C. P. Airborne Infrared Spectroscopy of 1994 Western Wildfires. *Journal of Geophysical Research: Atmospheres* **1997**, *102* (D1), 1287−1299.

(26) Johnson, D. G.; Jucks, K. W.; Traub, W. A.; Chance, K. V. Smithsonian Stratospheric Far-Infrared Spectrometer and Data Reduction System. *Journal of Geophysical Research: Atmospheres* **1995**, *100* (D2), 3091−3106.

(27) Blom, C. E.; Fischer, H.; Glatthor, N.; Gulde, T.; Höpfner, M.; Piesch, C. Spatial and Temporal Variability of ClONO2, HNO3, and O3 in the Arctic Winter of 1992/1993 as Obtained by Airborne Infrared Emission Spectroscopy. *Journal of Geophysical Research: Atmospheres* **1995**, *100* (D5), 9101−9114.

https://doi.org/10.1021/acsearthspacechem.1c00281
ACS Earth Space Chem. 2022, 6, 582−596

(28) Traub, W. A.; Jucks, K. W.; Johnson, D. G.; Coffey, M. T.; Mankin, W. G.; Toon, G. C. Comparison of Column Abundances from Three Infrared Spectrometers during AASE II. *Geophys. Res. Lett.* **1994**, *21* (23), 2591−2594.
(29) Coffey, M. T.; Hannigan, J. W. The Temporal Trend of Stratospheric Carbonyl Sulfide. *Journal of Atmospheric Chemistry* **2010**, *67* (1), 61−70.
(30) Mankin, W. G. Airborne Fourier Transform Spectroscopy of the Upper Atmosphere. *Optical Engineering* **1978**, *17* (1), 170139.
(31) Mankin, W. G.; Coffey, M. T. Airborne Measurements of Stratospheric Constituents over Antarctica in the Austral Spring 1987:1. Method and Ozone Observations. *Journal of Geophysical Research: Atmospheres* **1989**, *94* (D9), 11413−11421.
(32) Toon, G. C.; Blavier, J.-F.; Solario, J. N.; Szeto, J. T. Airborne Observations of the Composition of the 1992 Tropical Stratosphere by FTIR Solar Absorption Spectrometry. *Geophys. Res. Lett.* **1993**, *20* (22), 2503−2506.
(33) Volkamer, R.; Kille, N.; Lee, C.; Zarzana, K. J.; Koenig, T. K.; Howard, B.; Nutter, R.; Knote, C.; Campos, T. L.; Plummer, D. M.; Oolman, L.; Deng, M.; Wang, Z.; Ahmadov, R.; Pierce, R. B.; Zahn, A.; Obersteiner, F.; Goulden, T.; Hass, B.; Fischer, E. V.; Hudak, A. T.; Restaino, J.; Ottmar, R. D. The BB-FLUX project: How much fuel goes up in smoke? *American Meteorological Society Annual Meeting*; Boston, MA, Jan 12−16, 2020. https://ams.confex.com/ams/2020Annual/videogateway.cgi/id/522007?recordingid=522007.
(34) Theys, N.; Volkamer, R.; Müller, J.-F.; Zarzana, K. J.; Kille, N.; Clarisse, L.; De Smedt, I.; Lerot, C.; Finkenzeller, H.; Hendrick, F.; Koenig, T. K.; Lee, C. F.; Knote, C.; Yu, H.; Van Roozendael, M. Global Nitrous Acid Emissions and Levels of Regional Oxidants Enhanced by Wildfires. *Nature Geoscience 2020 13:10* **2020**, *13* (10), 681−686.
(35) Ortega, I.; Buchholz, R.; Hall, E. G.; Hurst, D. F.; Jordan, A. F.; Hannigan, J. W. Tropospheric Water Vapor Profiles Obtained with FTIR: Comparison with Balloon-Borne Frost Point Hygrometers and Influence on Trace Gas Retrievals. *Atmospheric Measurement Techniques* **2019**, *12* (2), 873−890.
(36) Baidar, S.; Kille, N.; Ortega, I.; Sinreich, R.; Thomson, D.; Hannigan, J.; Volkamer, R. Development of a Digital Mobile Solar Tracker. *Atmospheric Measurement Techniques* **2016**, *9* (3), 963−972.
(37) Hase, F.; Hannigan, J. W.; Coffey, M. T.; Goldman, A.; Höpfner, M.; Jones, N. B.; Rinsland, C. P.; Wood, S. W. Intercomparison of Retrieval Codes Used for the Analysis of High-Resolution, Ground-Based FTIR Measurements. *Journal of Quantitative Spectroscopy and Radiative Transfer* **2004**, *87* (1), 25−52.
(38) Viatte, C.; Strong, K.; Walker, K. A.; Drummond, J. R. Five Years of CO, HCN, C2H6, C2H2, CH3OH, HCOOH and H2CO Total Columns Measured in the Canadian High Arctic. *Atmospheric Measurement Techniques* **2014**, *7* (6), 1547−1570.
(39) Wunch, D.; Toon, G. C.; Blavier, J.-F. L.; Washenfelder, R. A.; Notholt, J.; Connor, B. J.; Griffith, D. W. T.; Sherlock, V.; Wennberg, P. O. The Total Carbon Column Observing Network. *Philosophical Transactions of the Royal Society A: Mathematical, Physical and Engineering Sciences* **2011**, *369* (1943), 2087−2112.
(40) Toon, O. B.; Tolbert, M. A. Spectroscopic Evidence against Nitric Acid Trihydrate in Polar Stratospheric Clouds. *Nature 1995 375:6528* **1995**, *375* (6528), 218−221.
(41) Höpfner, M.; Ungermann, J.; Borrmann, S.; Wagner, R.; Spang, R.; Riese, M.; Stiller, G.; Appel, O.; Batenburg, A. M.; Bucci, S.; Cairo, F.; Dragoneas, A.; Friedl-Vallon, F.; Hünig, A.; Johansson, S.; Krasauskas, L.; Legras, B.; Leisner, T.; Mahnke, C.; Möhler, O.; Molleker, S.; Müller, R.; Neubert, T.; Orphal, J.; Preusse, P.; Rex, M.; Saathoff, H.; Stroh, F.; Weigel, R.; Wohltmann, I. Ammonium Nitrate Particles Formed in Upper Troposphere from Ground Ammonia Sources during Asian Monsoons. *Nature Geoscience 2019 12:8* **2019**, *12* (8), 608−612.
(42) Permar, W.; Wang, Q.; Selimovic, V.; Wielgasz, C.; Yokelson, R. J.; Hornbrook, R. S.; Hills, A. J.; Apel, E. C.; Ku, I.-T.; Zhou, Y.; Sive, B. C.; Sullivan, A. P.; Collett, J. L.; Campos, T. L.; Palm, B. B.; Peng, Q.; Thornton, J. A.; Garofalo, L. A.; Farmer, D. K.; Kreidenweis, S. M.; Levin, E. J. T.; DeMott, P. J.; Flocke, F.; Fischer, E. V.; Hu, L. Emissions of Trace Organic Gases From Western U.S. Wildfires Based on WE-CAN Aircraft Measurements. *Journal of Geophysical Research: Atmospheres* **2021**, *126* (11), e2020JD033838.
(43) Apel, E. C.; Hornbrook, R. S.; Hills, A. J.; Blake, N. J.; Barth, M. C.; Weinheimer, A.; Cantrell, C.; Rutledge, S. A.; Basarab, B.; Crawford, J.; Diskin, G.; Homeyer, C. R.; Campos, T.; Flocke, F.; Fried, A.; Blake, D. R.; Brune, W.; Pollack, I.; Peischl, J.; Ryerson, T.; Wennberg, P. O.; Crounse, J. D.; Wisthaler, A.; Mikoviny, T.; Huey, G.; Heikes, B.; O'Sullivan, D.; Riemer, D. D. Upper Tropospheric Ozone Production from Lightning NOx-Impacted Convection: Smoke Ingestion Case Study from the DC3 Campaign. *Journal of Geophysical Research: Atmospheres* **2015**, *120* (6), 2505−2523.
(44) Hornbrook, R. S.; Blake, D. R.; Diskin, G. S.; Fried, A.; Fuelberg, H. E.; Meinardi, S.; Mikoviny, T.; Richter, D.; Sachse, G. W.; Vay, S. A.; Walega, J.; Weibring, P.; Weinheimer, A. J.; Wiedinmyer, C.; Wisthaler, A.; Hills, A.; Riemer, D. D.; Apel, E. C. Observations of Nonmethane Organic Compounds during ARCTAS-Part 1: Biomass Burning Emissions and Plume Enhancements. *Atmospheric Chemistry and Physics* **2011**, *11* (21), 11103−11130.
(45) Palm, B. B.; Peng, Q.; Fredrickson, C. D.; Lee, B. H.; Garofalo, L. A.; Pothier, M. A.; Kreidenweis, S. M.; Farmer, D. K.; Pokhrel, R. P.; Shen, Y.; Murphy, S. M.; Permar, W.; Hu, L.; Campos, T. L.; Hall, S. R.; Ullmann, K.; Zhang, X.; Flocke, F.; Fischer, E. V.; Thornton, J. A. Quantification of Organic Aerosol and Brown Carbon Evolution in Fresh Wildfire Plumes. *Proc. Natl. Acad. Sci. U. S. A.* **2020**, *117* (47), 29469−29477.
(46) Peng, Q.; Palm, B. B.; Melander, K. E.; Lee, B. H.; Hall, S. R.; Ullmann, K.; Campos, T.; Weinheimer, A. J.; Apel, E. C.; Hornbrook, R. S.; Hills, A. J.; Montzka, D. D.; Flocke, F.; Hu, L.; Permar, W.; Wielgasz, C.; Lindaas, J.; Pollack, I. B.; Fischer, E. V.; Bertram, T. H.; Thornton, J. A. HONO Emissions from Western U.S. Wildfires Provide Dominant Radical Source in Fresh Wildfire Smoke. *Environ. Sci. Technol.* **2020**, *54* (10), 5954−5963.
(47) Andrews, S. J.; Carpenter, L. J.; Apel, E. C.; Atlas, E.; Donets, V.; Hopkins, J. R.; Hornbrook, R. S.; Lewis, A. C.; Lidster, R. T.; Lueb, R.; Minaeian, J.; Navarro, M.; Punjabi, S.; Riemer, D.; Schauffler, S. A Comparison of Very Short Lived Halocarbon (VSLS) and DMS Aircraft Measurements in the Tropical West Pacific from CAST, ATTREX and CONTRAST. *Atmospheric Measurement Techniques* **2016**, *9* (10), 5213−5225.
(48) Zhou, Y.; Shively, D.; Mao, H.; Russo, R. S.; Pape, B.; Mower, R. N.; Talbot, R.; Sive, B. C. Air Toxic Emissions from Snowmobiles in Yellowstone National Park. *Environ. Sci. Technol.* **2010**, *44* (1), 222−228.
(49) Benedict, K. B.; Zhou, Y.; Sive, B. C.; Prenni, A. J.; Gebhart, K. A.; Fischer, E. V.; Evanoski-Cole, A.; Sullivan, A. P.; Callahan, S.; Schichtel, B. A.; Mao, H.; Zhou, Y.; Collett, J. L. Volatile Organic Compounds and Ozone in Rocky Mountain National Park during FRAPPÉ. *Atmospheric Chemistry and Physics* **2019**, *19* (1), 499−521.
(50) Zheng, W.; Flocke, F. M.; Tyndall, G. S.; Swanson, A.; Orlando, J. J.; Roberts, J. M.; Huey, L. G.; Tanner, D. J. Characterization of a Thermal Decomposition Chemical Ionization Mass Spectrometer for the Measurement of Peroxy Acyl Nitrates (PANs) in the Atmosphere. *Atmospheric Chemistry and Physics* **2011**, *11* (13), 6529−6547.
(51) Pollack, I. B.; Lindaas, J.; Roscioli, J. R.; Agnese, M.; Permar, W.; Hu, L.; Fischer, E. V. Evaluation of Ambient Ammonia Measurements from a Research Aircraft Using a Closed-Path QC-TILDAS Operated with Active Continuous Passivation. *Atmospheric Measurement Techniques* **2019**, *12* (7), 3717−3742.
(52) Gilman, J. B.; Lerner, B. M.; Kuster, W. C.; Goldan, P. D.; Warneke, C.; Veres, P. R.; Roberts, J. M.; De Gouw, J. A.; Burling, I. R.; Yokelson, R. J. Biomass Burning Emissions and Potential Air Quality Impacts of Volatile Organic Compounds and Other Trace Gases from Fuels Common in the US. *Atmospheric Chemistry and Physics* **2015**, *15* (24), 13915−13938.
(53) Garofalo, L. A.; Pothier, M. A.; Levin, E. J. T.; Campos, T.; Kreidenweis, S. M.; Farmer, D. K. Emission and Evolution of

Submicron Organic Aerosol in Smoke from Wildfires in the Western United States. *ACS Earth and Space Chemistry* **2019**, *3* (7), 1237−1247.
(54) Rogers, J. D.; Rhead, L. A. Peroxyglutaryl Nitrate: Formation and Infrared Spectrum. *Atmospheric Environment (1967)* **1987**, *21* (12), 2519−2523.
(55) Edney, E. O.; Spence, J. W.; Hanst, P. L. Synthesis and Thermal Stability of Peroxy Alkyl Nitrates. *Journal of the Air Pollution Control Association* **1979**, *29* (7), 741−743.
(56) Monedero, E.; Salgado, M. S.; Villanueva, F.; Martín, P.; Barnes, I.; Cabañas, B. Infrared Absorption Cross-Sections for Peroxyacyl Nitrates (NPANs). *Chem. Phys. Lett.* **2008**, *465* (4−6), 207−211.
(57) Roberts, J. M.; Marchewka, M.; Bertman, S. B.; Sommariva, R.; Warneke, C.; de Gouw, J.; Kuster, W.; Goldan, P.; Williams, E.; Lerner, B. M.; Murphy, P.; Fehsenfeld, F. C. Measurements of PANs during the New England Air Quality Study 2002. *Journal of Geophysical Research: Atmospheres* **2007**, *112* (D20), 20306.
(58) LaFranchi, B. W.; Wolfe, G. M.; Thornton, J. A.; Harrold, S. A.; Browne, E. C.; Min, K. E.; Wooldridge, P. J.; Gilman, J. B.; Kuster, W. C.; Goldan, P. D.; De Gouw, J. A.; McKay, M.; Goldstein, A. H.; Ren, X.; Mao, J.; Cohen, R. C. Closing the Peroxy Acetyl Nitrate Budget: Observations of Acyl Peroxy Nitrates (PAN, PPN, and MPAN) during BEARPEX 2007. *Atmospheric Chemistry and Physics* **2009**, *9* (19), 7623−7641.
(59) Juncosa Calahorrano, J. F.; Lindaas, J.; O'Dell, K.; Palm, B. B.; Peng, Q.; Flocke, F.; Pollack, I. B.; Garofalo, L. A.; Farmer, D. K.; Pierce, J. R.; Collett, J. L.; Weinheimer, A.; Campos, T.; Hornbrook, R. S.; Hall, S. R.; Ullmann, K.; Pothier, M. A.; Apel, E. C.; Permar, W.; Hu, L.; Hills, A. J.; Montzka, D.; Tyndall, G.; Thornton, J. A.; Fischer, E. V. Daytime Oxidized Reactive Nitrogen Partitioning in Western U.S. Wildfire Smoke Plumes. *Journal of Geophysical Research: Atmospheres* **2021**, *126* (4), e2020JD033484.
(60) Roiger, A.; Aufmhoff, H.; Stock, P.; Arnold, F.; Schlager, H. An Aircraft-Borne Chemical Ionization - Ion Trap Mass Spectrometer (CI-ITMS) for Fast PAN and PPN Measurements. *Atmospheric Measurement Techniques* **2011**, *4* (2), 173−188.
(61) Wolfe, G. M.; Thornton, J. A.; McNeill, V. F.; Jaffe, D. A.; Reidmiller, D.; Chand, D.; Smith, J.; Swartzendruber, P.; Flocke, F.; Zheng, W. Influence of Trans-Pacific Pollution Transport on Acyl Peroxy Nitrate Abundances and Speciation at Mount Bachelor Observatory during INTEX-B. *Atmospheric Chemistry and Physics* **2007**, *7* (20), 5309−5325.
(62) Andreae, M. O. Emission of Trace Gases and Aerosols from Biomass Burning - An Updated Assessment. *Atmospheric Chemistry and Physics* **2019**, *19* (13), 8523−8546.
(63) Prichard, S. J.; O'Neill, S. M.; Eagle, P.; Andreu, A. G.; Drye, B.; Dubowy, J.; Urbanski, S.; Strand, T. M. Wildland Fire Emission Factors in North America: Synthesis of Existing Data, Measurement Needs and Management Applications. *International Journal of Wildland Fire* **2020**, *29* (2), 132−147.
(64) Lindaas, J.; Pollack, I. B.; Garofalo, L. A.; Pothier, M. A.; Farmer, D. K.; Kreidenweis, S. M.; Campos, T. L.; Flocke, F.; Weinheimer, A. J.; Montzka, D. D.; Tyndall, G. S.; Palm, B. B.; Peng, Q.; Thornton, J. A.; Permar, W.; Wielgasz, C.; Hu, L.; Ottmar, R. D.; Restaino, J. C.; Hudak, A. T.; Ku, I.-T.; Zhou, Y.; Sive, B. C.; Sullivan, A.; Collett, J. L.; Fischer, E. V. Emissions of Reactive Nitrogen From Western U.S. Wildfires During Summer 2018. *Journal of Geophysical Research: Atmospheres* **2021**, *126* (2), e2020JD032657.
(65) Stockwell, C. E.; Jayarathne, T.; Cochrane, M. A.; Ryan, K. C.; Putra, E. I.; Saharjo, B. H.; Nurhayati, A. D.; Albar, I.; Blake, D. R.; Simpson, I. J.; Stone, E. A.; Yokelson, R. J. Field Measurements of Trace Gases and Aerosols Emitted by Peat Fires in Central Kalimantan, Indonesia, during the 2015 El Niño. *Atmospheric Chemistry and Physics* **2016**, *16* (18), 11711−11732.

Recommended by ACS

Mixing State of Carbonaceous Aerosols of Primary Emissions from "Improved" African Cookstoves
Yuchieh Ting, Hugh Coe, *et al.*
AUGUST 01, 2018
ENVIRONMENTAL SCIENCE & TECHNOLOGY
READ

Emissions of Gases and Volatile Organic Compounds from Residential Heating: A Comparison of Brown Coal Briquettes and Logwood Combustion
Patrick Martens, Ralf Zimmermann, *et al.*
AUGUST 19, 2021
ENERGY & FUELS
READ

PM2.5-Associated Health Impacts of Beehive Coke Oven Ban in China
Yang Xu, Shu Tao, *et al.*
SEPTEMBER 05, 2019
ENVIRONMENTAL SCIENCE & TECHNOLOGY
READ

Top-Down Determination of Black Carbon Emissions from Oil Sand Facilities in Alberta, Canada Using Aircraft Measurements
Yuan Cheng, Mengistu Wolde, *et al.*
DECEMBER 13, 2019
ENVIRONMENTAL SCIENCE & TECHNOLOGY
READ

Get More Suggestions >

https://doi.org/10.1021/acsearthspacechem.1c00281
ACS Earth Space Chem. 2022, 6, 582−596